

MICHIGAN STATE UNIVERSITY LIBRARIES
3 1293 00564 9656

22098289

LIBRARY Michigan State University

This is to certify that the

thesis entitled

EXPERIMENTAL INVESTIGATION OF NONLINEAR OSCILLATIONS OF A BASE EXCITED FLEXIBLE CANTILEVER BEAM

presented by

Syed Masroor Hasan

has been accepted towards fulfillment of the requirements for

M.S. degree in Mechanical Engineering

Major professor

Date 2/20/89

O-7639

MSU is an Affirmative Action/Equal Opportunity Institution



RETURNING MATERIALS:
Place in book drop to remove this checkout from your record. FINES will be charged if book is returned after the date

returned after the stamped below.

EXPERIMENTAL INVESTIGATION OF NONLINEAR OSCILLATIONS OF A BASE EXCITED FLEXIBLE CANTILEVER BEAM

 $\mathbf{B}\mathbf{y}$

Syed Masroor Hasan

A THESIS

Submitted to

Michigan State University
in partial fulfillment of the requirements

for the degree of

MASTER OF SCIENCE

Department of Mechanical Engineering
1989

ABSTRACT

Experimental Investigation of Nonlinear
Oscillations of a Base Excited
Flexible Cantilever Beam.

By

Syed Masroor Hasan

A study is made of the nonlinear response of a flexible cantilever beam excited by a sinusoidal base motion. Experimental results are presented which exhibit a variety of unusual and potentially dangerous phenomena such as chaos, multi-mode interaction, multiple steady-states and a very high order subharmonic response. Particular attention is focused on resonances which can occur at frequencies well removed from the excitation frequency. In addition, the partial integro-differential equation is obtained which governs the planar motion of the beam. It takes into account the effects of large curvature and axial deformations and includes up to order three nonlinearities. For a single mode response, the equation can be reduced to Mathieu's equation with a cubic nonlinearity. The stability of the trivial solution of this equation is studied using a perturbation technique and the results are compared to experimentally obtained data. In conclusion, the pointwise dimension is estimated for the chaotic motion observed, and the results suggest that the chaotic motion can be modelled by three orthogonal modes.

Dedicated to my father, Syed Ghiasul Haq.

ACKNOWLEDGMENTS

I would like to express my sincere gratitude to Dr. Alan Haddow, my major professor, for his patient guidance and assistance during the period of research and graduate study. It has enhanced the content of this thesis considerably.

The other members of my Master Committee also deserve my thanks. Drs. Clark Radcliffe and Joe Whitesell were all helpful, and their comments and observations concerning this work were very useful.

Special thanks to Bob Rose from the machine shop for his valuable aid in the construction of the experimental set-up.

My family has been a source of strength, love, and moral support for me, especially over the last two years. I only hope that I can put back as much as I have drawn. To my father and mother, Ghias and Rabia, my brothers and sisters, Masood, Shahida, Mahmood, Rukhsana, and Sarwat... thank you, I couldn't have done it without you. I would also like to thank my fiancee Lubna, and her family, for their patience and understanding.

Finally a sincer thanks to my friends. I would especially like to thank Brian D'Mello, and Mohammad Usman for their extra support and help. To all my other friends, thanks for being there when I needed you.

Table of Contents

List Of Tables	vi
List of Figures	vii
Chapter 1: Introduction	1
1.1: Scope of the Work	1
1.2: Literature Review	2
Chapter 2: The Governing Equation for Planar Motion	4
Chapter 3: Stability Analysis	11
3.1: Introduction	11
3.2: Reduction to Mathieu's Equation	11
3.3: Stability Analysis	12
Chapter 4: Experimental Results	16
4.1: Experimental Set-up	16
4.2: Linear Stability and Planar Steady-State Motion	16
4.3: Chaos	22
4.3.1: Transient Chaos	27
4.3.2: Intermittent and Steady-State Chaos	28
4.4: Multi-Mode Interaction	35
4.4.1: Extremely Low Sub-harmonic Response	35
4.4.2: Modal Interaction and Beating Phenomenon	39
4.4.3: Combination Resonance	42
Chapter 5: Dimension Estimate	45
5.1: Introduction	45
5.2: Acquisition of Data	48
5.3: Estimation of Optimal Time Delay	48
5.4: Reconstructed Coordinates and Dimension Estimate	52
5.5: Conclusions	58
Chapter 6: Conclusions	59
Appendix A	61
Appendix B	62
List of References	63

List of Tables

Table 2.1: Values of r_j and r_j	K_j)
Table 2.2: Values of β_i, γ_i, i	and λ_j 10	J

List of Figures

Figure 2.1: Cantilever beam and coordinate system	5
Figure 2.2: Angle of rotation of a differential element of beam	5
Figure 3.1: Transition curves seperating stable and unstable regions	15
Figure 4.1: Sketch of existing experimental set-up	17
Figure 4.2: Block diagram of the experimental set-up	18
Figure 4.3: Stability diagram for fourth mode	20
Figure 4.4: Comparision of theoretical Strutt diagram with experimental data points for fourth mode	21
Figure 4.5a: Sketch of frequency reponse curve for nonlinear Mathieu's equation.	23
Figure 4.5b: Experimental frequency response curve.	23
Figure 4.6: Time trace showing a steady-state parametric response	24
Figure 4.6: FFT of time trace	25
Figure 4.7: Experimental frequency response curve. Level of force constant but higher than Figure 4.5b	26
Figure 4.8: Transient chaotic response for a forcing frequency of 87.0 Hz	29
Figure 4.9: Robust chaotic response for a forcing frequency of 87.0 Hz	31 32
Figure 4.10: Steady-state parametric response for a forcing frequency of 45.0 Hz	33
Figure 4.11: Chaotic response for a forcing frequency of 43 Hz	34
Figure 4.12: Time traces for initial time close to zero at 195 Hz.	36
Figure 4.13: Time traces at time t+30 secs at 195 Hz	37
Figure 4.14: FFT of time trace at t+30 secs	38
Figure 4.15: Waterfall plot showing output close to an initial time zero at 385.6 Hz	40
Figure 4.16: Waterfall plot showing output some t+10 secs later for a forcing frequency of 385.6 Hz	4]
Figure 4.17: Combination of responses at a forcing frequency of 85.5 Hz	43
Figure 4.18: Chaotic response for a forcing frequency of 85.5 Hz	
Figure 5.1: Flow chart for dimension estimate	49
Figure 5.2: The unnormalized autocorrelation function for various time delays	5 1
Figure 5.3: Phase portrait of measured time signal SGS (t) from cantil- ever beam using the reconstructed coordinates	53
Figure 5.4a: log P plotted against log r for m = 3.9 and 15	

Figure 5.4b: The embedding dimension m plotted against the pointwise	
dimension of the attractor	57
Figure A.1: An element of beam	66

CHAPTER 1

INTRODUCTION

1.1 Scope of the Work

Recently, there has been a growing interest in the dynamical behaviour of flexible structures. Such structures are becoming more common as designers are continually striving to make efficient use of newly available materials and make lighter, less expensive products. There is often the need to reduce the weight to a bare minimum, in order to reduce the inertial loading on the system. This is particularly desirable if the application involves high speed machinery e.g. robot arms. Another area in which flexibility is a problem is that of space structures. In a zero gravity environment a structure does not have to be designed to withstand its own weight. The resulting designs are often very flexible.

The main aim of this work is to experimentally investigate the dynamical behaviour of a flexible structure. A relatively simple model is chosen, viz. a cantilever beam of dimensions 55.88 cm x 1.27 cm x 0.0508 cm and it is excited by a sinusoidal base motion in the longitudanal direction. Chapter 4 catalogues the various types of vibration phenomena observed. A number of these have received attention in the past, such as main parametric resonances, multiple steady-states and the jump phenomenon. However, less well documented behaviour was also observed, including chaotic response, multi-mode interactions and very high order sub-harmonic responses.

Before discussing the experimental observations, the governing equation of motion of the system is derived in Chapter 2. It is valid for in-plane motions with large curvatures and it includes up to third order nonlinear terms. In this thesis, limited use is made of the equation of motion, but it will act as a sound starting point for future studies in this area. The equation is also used to predict the

theoretical stability of the trivial solution. This is undertaken in Chapter 3 and the results are compared with the experimental results in Chapter 4.

Chapter 5 is concerned with a more detailed study of the chaotic response. A discussion is presented as to the use of dimension calculations and and such a calculation is undertaken for the chaotic motion observed in the cantilever.

1.2 Literature Review

A review article by Sathyamoorthy [1982] surveys recent advances in the area of nonlinear analysis of beams. Most of the works dealing with planar motion are devoted to the study of axially restrained simply supported beam which take into account the nonlinearities due to mid-plane stretching. See, for example Wojnowsky Kreiger [1950], Evensen [1968], Ray and Bert [1969], Mei [1973], Nayfeh et al. [1974], and Bhashyam and Prathap [1980]. A few studies have dealt with the oscillations of beams with no axial restraint in which the nonlinearities arising from the effects of large curvature and longitudinal inertia are also considered, see Wagner [1965], Alturi [1973], and Luongo et al. [1986].

There have been a number of works related to the non-planar response of beams. For example, Crespo da Silva and Glynn [1978a] investigated the bending-bending-torsion of a beam. In part two of the paper, Crespo da Silva and Glynn [1978b], they extended the work to include the effects of a transverse force. Ho et al. [1975, 1976] studied a similar problem but did not consider the torsional motion. Hyer [1980] investigated the non-planar response of a base excited cantilever using the method of multiple scales, and presented numerical results for a specific beam excited near its fundamental and its second natural frequencies. Luongo et al. [1984a] considered the free non-planar motions of an inextensible elastic beam, supported in an arbitary manner without any axial restraints. A thorough mathematical investigation of Euler's elastica has been completed by Caflish and Maddocks [1984].

Tseng and Dugundji [1971] reported on what seems to be the first observation of chaotic motion in a physical structure. They completed a theoretical and an experimental investigation of the bending response of a buckled beam subjected to a harmonic excitation. Although it was not named as chaos a "snapthrough" response was observed both numerically and experimentally. The work was later expanded to include torsional responses, Dugundji and Mukhopadhyay [1973]. The text by Evan-Iwanowski [1976] reports on a number of experimental results relating to the steady-state, or almost steady-state response of beams. Evensen and Evan-Iwanowski [1966] investigated the stability of a column subjected to axial excitation. Handoo and Sundararajan [1971] studied a similar problem. Haight and King [1969] investigated planar and the non-planar stability of a rod due to an axial excitation. In a related work, Haight and King [1971] studied a similar problem but with a lateral excitation. Takahski [1979] reported on the stability of multi-mode, steady-state, planar response of a nonlinear beam. Dowell et al. [1977] devised an experiment to investigate the dependence of the bending and torsional natural frequencies on the static deflection of a hingless rotor blade A detailed investigation by Bux and Roberts [1986] reported on the complex modal interactions that can occur as a consequence of internal resonances. They studied both theoretically and experimentally, the behaviour of a system of coupled beams. Housner and Belvin [1986] studied the transient response of a slender guyed boom.

Works reporting on the experimental existence of chaos in structures include those by Moon and Holmes [1979], Moon [1980], Shaw [1985] and Burton & Kolowith [1988].

CHAPTER 2

THE GOVERNING EQUATION FOR PLANAR MOTION

The planar vibration of a base excited cantilever beam is studied. The equation of motion is derived using Hamilton's Principle (see Goldstein [1980] pp 35-37), and terms arising from large curvature and from the resulting axial deflections are included. The equation of motion contains nonlinearities up to order three. Galerkin's method is used to reduce the partial differential equation of motion to a nonlinear ordinary differential equation by making use of the eigenfunctions of the linearized system.

The following assumptions are made to simplify the problem,

- i) the beam is inextensible,
- ii) there is no warping or shear deformation,
- iii) the effects of rotary inertia are neglected,

and

iv) the cross-sectional dimensions and the material properties of the beam are constant along the length.

Consider a slender beam of length l and mass m per unit length as shown in Figure 2.1. The base of the beam is located at the origin of the coordinate axes and has a known harmonic displacement in the x-direction of $b\sin(\Omega_l t)$, b being the magnitude of the displacement and Ω_l the excitation frequency. Let S be the path coordinate measured along the undeformed arc center line. For the planar motion, the deformed shape of the beam is defined by a displacement of w(S,t) and v(S,t) in x and y direction respectively, and by a rotation of the beam's cross section of $\theta(S,t)$.

Noting assumption (iii) and (iv), the total kinetic energy of the beam is given by,

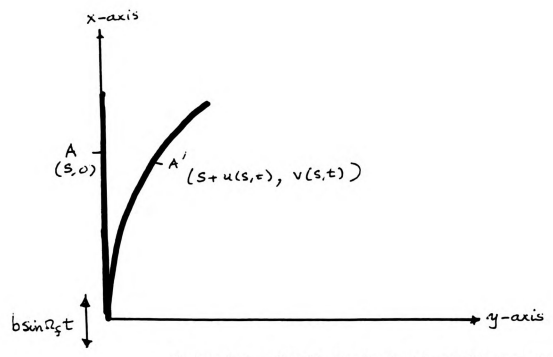


Figure 2.1: Cantilever beam and coordinate system

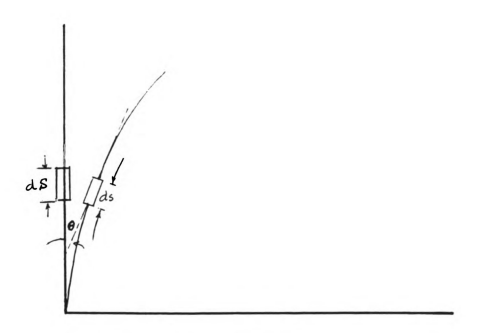


Figure 2.2: Angle of retation of a differential element of beam.

$$T(t) = \int_{0}^{t} \frac{1}{2} m(\dot{u}^{2}(S,t) + \dot{v}^{2}(S,t)) dS$$
 (2.1)

where a dot denotes partial differentiation with respect to the time t and m is the mass per unit length.

Noting assumption (i), the total potential energy of the beam is the elastic potential energy due to bending, and employing the usual notation, is given by,

$$V(t) = \int_{0}^{t} \frac{1}{2} EI \ \mu^{2}(S,t) \ dS \tag{2.2}$$

In the above equation, μ is the curvature of the center line.

The Lagrangian function (see Meirovitch [1967] pp 44) is given by

$$L(t) = T(t) - V(t)$$

$$L(t) = \int_{0}^{t} \left[\frac{1}{2} m \left(\dot{u}^{2} + \dot{v}^{2} \right) - \frac{1}{2} EI \mu^{2} \right] dS \qquad (2.3)$$

We now seek to express $\mu(S,t)$ in terms of the displacement component v(S,t). From assumption (ii) and Figure 2.2, the rotation $\theta(S,t)$ is related to the displacement derivatives by

$$\tan \theta = \frac{v'}{1+v'} \tag{2.4}$$

where the prime denotes the partial differentiation with respect to S. The expression for the strain (see Appendix A) in terms of displacement components is

$$\epsilon(S,t) = [(1+u')^2 + v'^2]^{1/2} - 1$$
 (2.5)

Expanding this using the Taylor series we get,

$$\epsilon(S,t) = u' + \frac{1}{2}v'^2$$
 (2.6)

Noting assumption (i), equation (2.6) reduces to

$$\mathbf{u}' = -\frac{1}{2} v'^2 \qquad (2.7)$$

The curvature expression is given by,

$$\mu(S,t) = \theta'(S,t) \tag{2.8}$$

Using equation (2.4) and equation (2.7) the curvature can be written as (see Appendix B)

$$\mu(S,t) = \theta'(S,t) = v''(1 + \frac{1}{2}v'^2)$$
 (2.9)

Substituting equation (2.9) into equation (2.3) yields

$$L(t) = \int_{0}^{t} \left[\frac{1}{2} m \left(\dot{u}^{2} + \dot{v}^{2} \right) - \frac{1}{2} EI \left(v'' \left(1 + \frac{1}{2} v'^{2} \right) \right)^{2} \right] dS$$
 (2.10)

The partial differential equations of motion can now be obtained by using the Hamilton's principle (see Goldstein [1980] pp 36), which requires that

$$\delta \int_{t_1}^{t_2} \int_{0}^{t} L(t) = 0$$

$$\delta \int_{t_1}^{t_2} \int_{0}^{t} \left[\frac{1}{2} m \left(\dot{u}^2 + \dot{v}^2 \right) - \frac{1}{2} EI \left(v'' \left(1 + \frac{1}{2} v'^2 \right) \right)^2 \right] dS = 0 \quad (2.11)$$

After taking variations with respect to u and v, performing integration by parts of the terms in equation (2.11), and rewriting them as the coefficients of variations δu and δv , which must vanish so that equation (2.11) holds, we arrive at:

$$\int_{t_1}^{t_2} \int_{0}^{1} \left[(-m\ddot{u})\delta u + (-m\ddot{v} - EI(v'''' + v'''' v'' + 4v'v'' v''' + v'''^3))\delta v \right] dS = 0$$
 (2.12)

In order to eliminate the function u(S,t) from the above equation, we integrate equation (2.7) with respect to S to obtain

$$\mathbf{z} (S,t) = \mathbf{z} (0,t) - \int_{0}^{S} \frac{1}{2} v'^{2} dS \qquad (2.13)$$

At the base of the beam (S=0), the u displacement is given by $u(0,t) = b\sin(\Omega_f t)$, hence

$$u(S,t) = b\sin(\Omega_f t) - \frac{1}{2} \int_0^S v'^2 dS$$
 (2.14)

Therefore

$$\ddot{u} = -\left(\frac{1}{2} \int_{0}^{S} v^{\prime 2} dS\right) - b \Omega_{f}^{2} \sin \left(\Omega_{f} t\right)$$
 (2.15)

Substituting equations (2.14) and (2.15) into equation (2.12) we get

$$\int_{t_1}^{t_2} \int_{0}^{l} \left[-mv' \left(\frac{1}{2} \int_{0}^{S} v'^2 dS \right) + mv'' \left(\int_{S}^{l} \left(\frac{1}{2} \int_{0}^{S} v'^2 dS \right) \right) \right]$$

$$mb \Omega_{f}^{2} \sin(\Omega_{f} t) \left[(l-S)v'' - v' \right]$$

$$(-mv - EI \left(v'''' + v'''' v'^2 + 4v' v'' v''' + v''^2 \right) \delta v \right] dS = 0$$
 (2.16)

The stationary condition leads to the partial governing integro-differential equation which determines v(S,t). The equation is

$$m\ddot{v} + EI \left(v'''' + v'''' v'^2 + 4v' v'' v''' + v''^3 \right) + mv' \left(\frac{1}{2} \int_0^S v'^2 dS \right) - mv'' \left(\int_S^I \left(\frac{1}{2} \int_0^S v'^2 dS \right) \right)$$

$$= mb \Omega_f^2 \sin(\Omega_f t) \left[(l - S)v'' - v' \right] \qquad (2.17)$$

Introducing the following non-dimensional terms,

$$\tilde{S} = \frac{S}{l} \qquad \tilde{t} = \omega t \qquad (where \, \omega = (\frac{EI}{ml^4})^{1/2})$$

$$\tilde{\Omega} = \frac{\Omega_f}{\omega} \qquad \tilde{b} = \frac{b}{l} \qquad (2.18)$$

we can non-dimensionalize equation (2.17). Dropping tilde for convenience, we get

$$\ddot{v} + v'''' + v''''v''^2 + 4v'v''v''' + v''^3 + v'(\frac{1}{2}\int_0^S v'^2 dS)$$

$$v''[\int_S (\frac{1}{2}\int_0^S v'^2 dS)dS] = b\Omega^2 \sin(\Omega t)[(1-S)v'' - v'] \qquad (2.19)$$

where dots and primes represent partial derivatives with respect to the new time \tilde{t} and new arc length \tilde{S} respectively.

The Galerkin's Method (see Meirovitch [1967]) can be used to reduce equation (2.19) to a ordinary differential equation. The displacement v(S,t) is assumed to be an eigenfunction of the linearized system, and a solution is sought of the form

$$v(S,t) = \phi_i(S)q_i(t)$$
 (2.20)

where j = 1,2,3....

The mode shape $\phi_j(S)$ of the linearized system is given by (see, for example Thompson [1981] pp 218-221),

$$\phi_j(S) = \cosh(r_j S) - \cos(r_j S) - K_j(\sinh(r_j S) - \sin(r_j S))$$
 (2.21)

where

$$K_j = \frac{\cosh(r_j S) + \cos(r_j S)}{\sinh(r_j S) + \sin(r_j S)}$$
(2.22)

The values of r_i and K_i as tabulated by Young and Felgar [1949] are as follows:

Table 2.1 Values of K_i and r_i

j	K_{j}	r_j
1	0.7341	1.8751
2	1.0185	4.6941
3	0.9992	7.8548
4	1.0000	10.99554

The substitution of equation (2.20) into equation (2.19) results in

$$q_{j}\phi_{j} + q_{j}\phi_{j}'''' + q_{j}^{3}[\phi_{j}''''\phi_{j}''^{2}+4\phi_{j}'\phi_{j}''\phi_{j}'''+\phi_{j}''$$

$$+q_{j}(q_{j}q_{j}+q_{j}^{2})(\phi_{j}'\int_{0}^{S}\phi_{j}'^{2}dS-\phi_{j}''\int_{0}^{1}(\int_{0}^{S}\phi_{j}'^{2}dS)dS)$$

$$=b\Omega^{2}\sin(\Omega t)[(1-S)\phi_{j}''-\phi_{j}'] \qquad (2.23)$$

An application of the Galerkin Method in the usual manner leads to the ordinary differential equation of the motion,

$$\ddot{q_j} + (\alpha_j + \beta_j b \Omega^2 \sin(\Omega t)) q_j + \gamma_j q_j^3 + \lambda_j [q_j^2 q_j^2 + q_j q_j^2] = 0$$
 (2.24)

The constants which appear in equation (2.24) are defined by

$$\alpha_{j} = \int_{0}^{1} \phi_{j}''''(S)\phi_{j}(S)dS = \tau_{j}^{4} \qquad (2.25a)$$

$$\gamma_{j} = \int_{0}^{1} (\phi_{j}'''' \phi_{j}''^{2}\phi_{j} + 4\phi_{j}' \phi_{j}'' \phi_{j}''' \phi_{j} + \phi_{j}''^{3}\phi_{j})dS \qquad (2.25b)$$

$$\lambda_{j} = \int_{0}^{1} [\phi_{j}'(\int_{0}^{S} \phi_{j}'^{2}dS) - \phi_{j}''(\int_{S} (\int_{0}^{S} \phi_{j}'^{2}))\phi_{j}dS \qquad (2.25c)$$

$$\beta_{j} = -\int_{0}^{1} [(1-S)\phi_{j}'' - \phi_{j}']\phi_{j}dS \qquad (2.25d)$$

The constants α_j , β_j , γ_j , and λ_j can be obtained by numerical integration of equations (2.25). For j = 1-4, these evaluate to:

Table 2.2 Values of β_j , γ_j , and λ_j

j	$\boldsymbol{\beta_j}$	γ_{j}	λ_j
1	1.57	40.44	4.60
2	8.65	13.4x10 ³	145
3	25.00	26.4x10 ⁴	10 ³
4	50.21	1.75x10 ⁶	3.65x10 ³

CHAPTER 3

STABILITY ANALYSIS

3.1 Introduction

The governing equation for planar motion obtained previously admits a trivial solution $(q_i(t)=0)$. In this section we study the stability of this solution for a main parametric resonance, i.e for a forcing frequency in the region of twice the natural frequency. The boundaries between stable and unstable solutions are obtained using Lindstedt-Poincare Method. The method is explained in detail in Nayfeh & Mook [1979] (pp 54-56) and only those steps pertinent to this particular problem will be included here.

3.2 Reduction to Mathieu's Equation

Recalling equation (2.24), the general equation of motion is

$$\ddot{q}_{j} + (\alpha_{j} + \beta_{j} b \Omega^{2} \sin(\Omega t)) q_{j} + \gamma_{j} q_{j}^{3} + \lambda_{j} (q_{j}^{2} \ddot{q}_{j} + q_{j} \dot{q}_{j}^{2}) = 0$$

Since the stability of the trivial solution is sought we can drop the nonlinear terms, which yields

$$\ddot{q}_j + (\alpha_j + \beta_j b \Omega^2 \sin(\Omega t)) q_j = 0$$
 (3.1)

The above equation is now reduced to the form whose stability has been studied by Nayfeh & Mook [1979] (pp 300-301). Let $\bar{t} = \frac{\Omega}{2}t$ and substitute this into equation 3.1, noting that the dots are now derivatives with respect to new time \bar{t} , we get

$$\ddot{q}_j + \left[\frac{4\alpha_j}{\Omega^2} + 4\beta_j b \sin(2\bar{t})\right] q_j = 0 \qquad (3.2)$$

Let

$$\delta = \frac{4\alpha_j}{\Omega^2} \tag{3.3a}$$

and

$$\epsilon_j = 2\beta_j b \qquad (3.3b)$$

and dropping the over bar for convenience, the equation 3.2 becomes

$$\ddot{q}_j + (\delta + 2\epsilon_j \sin(2t)) q_j = 0 \tag{3.4}$$

which is the standard form of Mathieu's equation.

3.3 Stability Analysis

The stability analysis is carried out using Lindstedt-Poincare technique which is valid for small ϵ ($\epsilon \approx 0.035$ in our case). Before application of the method, a damping term should be introduced into equation (3.4) to account for small energy losses in the physical system. The general form of the stability diagram is not affected by the value of the damping coefficient, provided the damping is small. The system we are considering is very lightly damped. Therefore, instead of accurately modelling the damping, we will assume it to be viscous with a coefficient, $\epsilon_{ij}\mu$, of 0.001. Even if we choose ten times higher damping coefficient, it results in altering the boundaries between stable and unstable regions, by less than 1%. Adding this to equation (3.4) and dropping subscript j for convenience results in

$$\ddot{q} + (\delta + 2\epsilon \sin(2t))q + 2\mu\epsilon \dot{q} = 0$$
 (3.5)

Now we will follow the method as outlined by Nayfeh & Mook [1979] (pp 300-301), to obtain boundaries between the stable and unstable regions. Using a first order approximation, let

$$q(t:\epsilon)=q_0(t)+\epsilon q_1(t)$$

$$\delta(\epsilon) = 1 + \epsilon \delta_1$$

Substituting these into equation (3.5) results in

$$(q_0+\epsilon q_1)+[(1+\epsilon \delta_1)+(2\epsilon \sin(2t))](q_0+\epsilon q_1)+2\epsilon \mu(q_0+\epsilon q_1)=0$$

Equating like powers of ϵ , we get

 ϵ^0 :

 ϵ^1 :

$$\dot{q}_1 + q_1 = -[\delta_1 + 2\sin(2t)]q_0 - 2\mu\dot{q_0} \tag{3.6b}$$

The solution of equation (3.6a) is

$$q_0 = a_0 \cos(t) + b_0 \sin(t)$$

Substituting this back into equation (3.6b) we get

$$\ddot{q_1+q_1} = -[\delta_1 + 2\sin(2t)][a_0\cos(t) + b_0\sin(t)] - 2\bar{\mu}\dot{u}_0[b_0\cos(t) - a_0\sin(t)]$$

and expanding the terms in the above equation, we get

Now eliminating secular producing terms, we get

$$\delta_1 a_0 + (1 + 2\mu) b_0 = 0 \tag{3.7a}$$

$$(1-2\mu)a_0+\delta_1b_0=0 (3.7b)$$

For a non-trivial solution to exist

$$\delta_1 = 1 + 2\mu 1 - 2\mu = 0$$

$$\delta_1^2 - (1 - 4\mu^2) = 0$$

$$=> \delta_1 = \pm \left[1 - 4\mu^2\right]^{1/2} \tag{3.8}$$

The transition curves seperating stable regions from unstable region are

$$\delta = 1 + \epsilon \, \delta_1$$

$$= > \qquad \delta = 1 \pm \left[\epsilon^2 - 4(\epsilon \mu)^2 \right]^{1/2} \tag{3.9}$$

These are approximate transition curves separating stable region from unstable region in $\delta - \epsilon$ space as shown in Figure 3.1. They hold for any single mode response (j=1,2,3...). In the next chapter we shall compare this theoretical result to the experimentally obtained stability boundaries for the fourth mode.

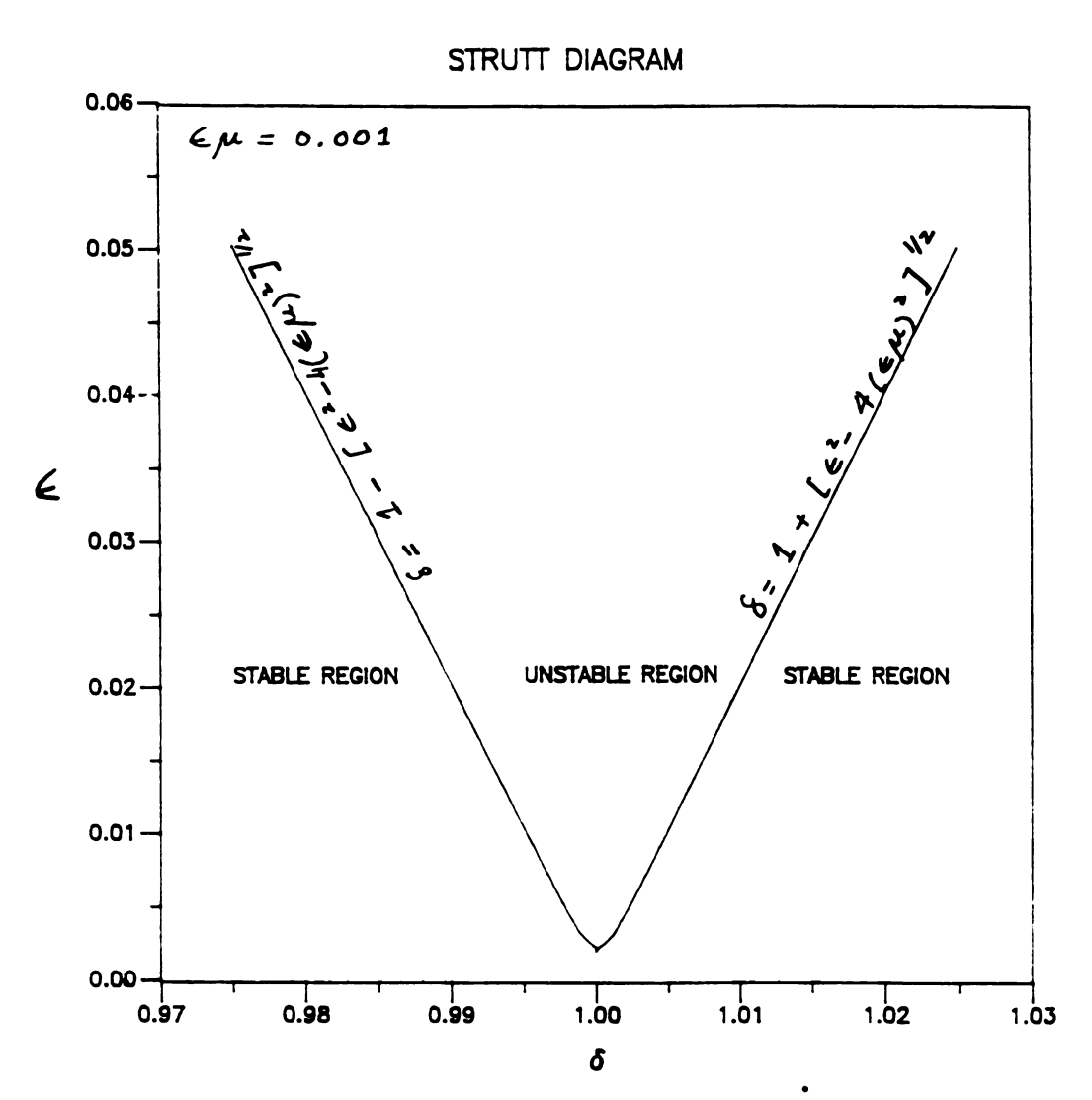


Figure 3.1: Transition curves seperating stable and unstable regions.

CHAPTER 4

EXPERIMENTAL RESULTS

4.1 Experimental Set-up:

A sketch of the existing experimental set-up is shown in Figure 4.1. The test specimen consists of a flexible steel cantilevered beam attached to a B&K type 4808 electromagnetic shaker. The beam is forced through a sinusoidal base excitation in the axial direction. The acceleration of this motion is proportional to the magnitude of the forcing term, $|\beta_j b\Omega^2|$ as it appears in equation (2.24). It is measured by an accelerometer attached to the head of the shaker.

The response of the beam is measured by two strain gages attached near the root of the cantilever. They are positioned on each side of the beam and can detect both in-plane and out-of-plane motions. The signals from the accelerometer and strain gages are analyzed and recorded on a HP 5423A structural dynamic analyzer. A block diagram of the experimental set-up is shown in Figure 4.2.

The first five linear natural frequencies associated with a motion in the x-y plane (i.e a transverse vibration in the flexible direction) were measured as $\Omega_1 = 1.0 \text{ Hz}$, $\Omega_2 = 8.0 \text{ Hz}$, $\Omega_3 = 22.5 \text{ Hz}$, $\Omega_4 = 44.8 \text{ Hz}$, and $\Omega_5 = 72 \text{ Hz}$. These compare well with the theoretical, linear natural frequency values of 1.24 Hz, 7.75 Hz, 21.74 Hz, 42.63 Hz and 70.47 Hz respectively (see, for example, Hartog [1980] pp 153, 432).

4.2 Linear Stability and Planar Steady State Motions

It is well documented that the dynamic stability of a beam excited by a sinusoidal displacement in the axial direction is given by a Strutt diagram (see Haight & King [1969]). In the displacement-frequency parameter space there are wedge shaped boundaries which separate the stable and unstable regions. The

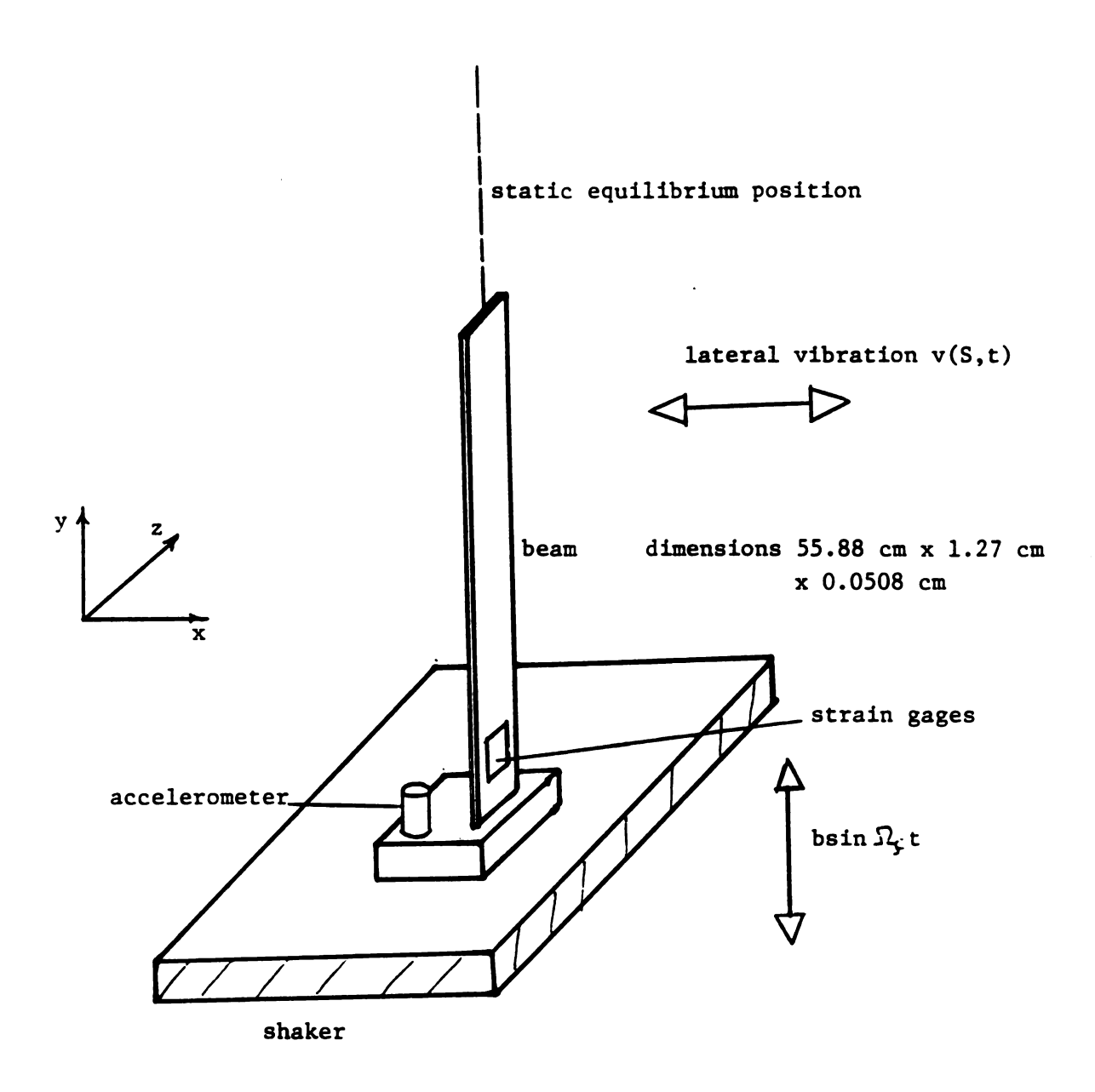


Figure 4.1: Sketch of existing experimental set-up

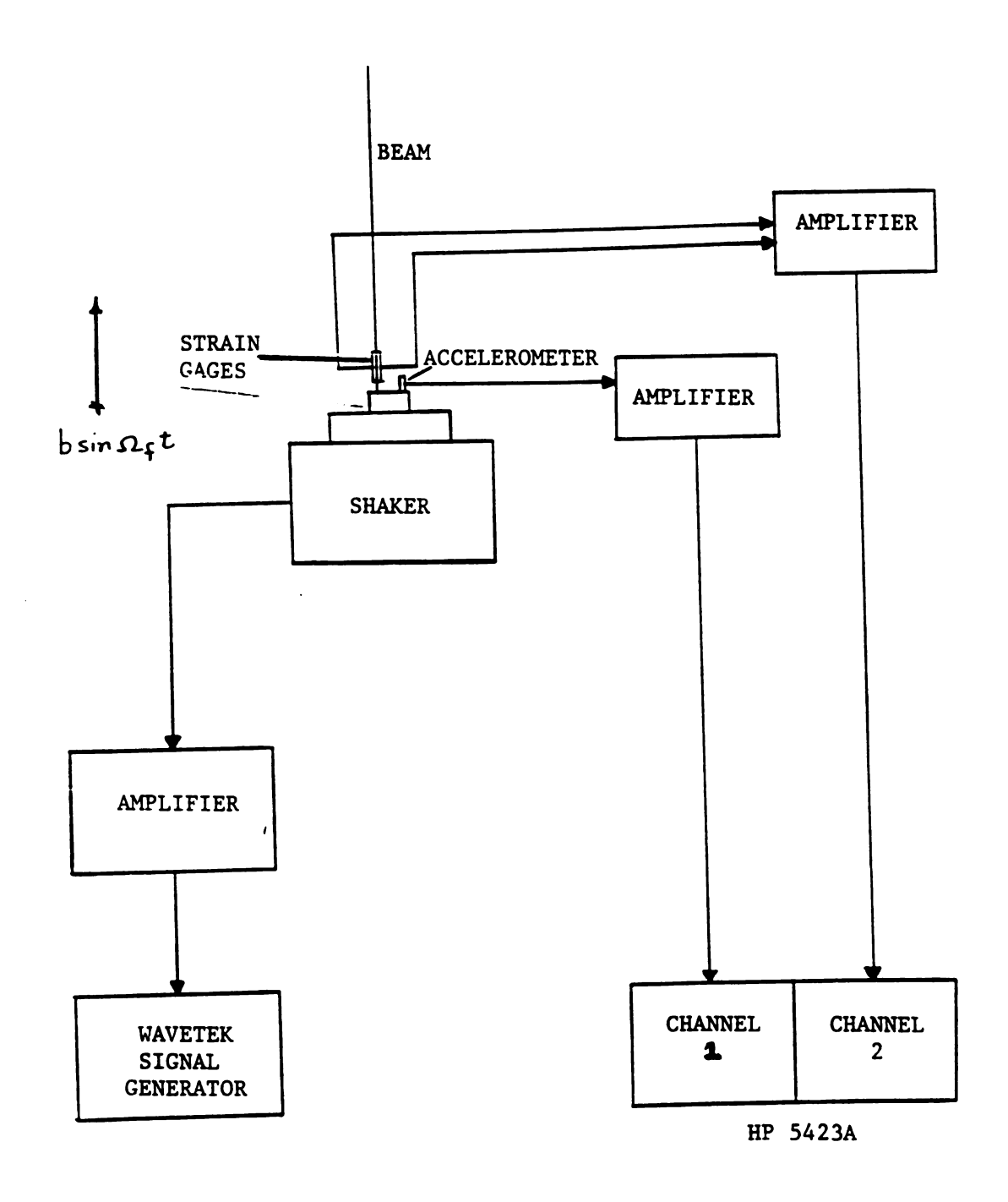


Figure 4.2: Block diagram of the experimental set-up

nose of these regions occur at forcing frequencies that are equal to twice the linear natural frequencies of the system (see Chapter 3). They also occur at multiples and combinations of these natural frequencies.

Figure 4.3 presents experimental data which defines one of these regions for the cantilever beam. It is associated with instability of the fourth in-plane mode of the system which results from a forcing frequency in the region of 89.6 Hz. Similar results can be obtained for other modes. The level of force corresponds to a range in the base acceleration between zero and 40 m/s^2 . The data points correspond to a transition from a trivial response to a non-trivial response.

Figure 4.4 presents a comparision of the experimental data with the theoretical Strutt diagram, obtained using equation (3.9). The comparision can be made by noting the following relationships for mode 4 from equations (3.3a) and (3.3b), and recalling from equation (2.25a) that $\alpha_4 = r_4^4$,

$$\delta = \frac{4r_4^4}{\Omega^2}$$

$$\epsilon_4 = 2\beta_4 b$$

where

 r_4 =10.99554 from table 2.1

 β_4 =50.21 from table 2.2

It should be noted that the experimental natural frequency is used in place of the theoretical linear natural frequency, to transform the experimental values of the forcing frequency to the variable δ . The experimental data points compare reasonably well with the theoretical predictions.

One should recall that the stability diagram presented in Figure 4.3 only predicts what happens to the trivial solution. Linear theory, which is valid for the trivial case, predicts that the trivial solution will grow exponentially in an unstable region (see, for example Nayfeh & Mook [1979] pp 338). However, as the

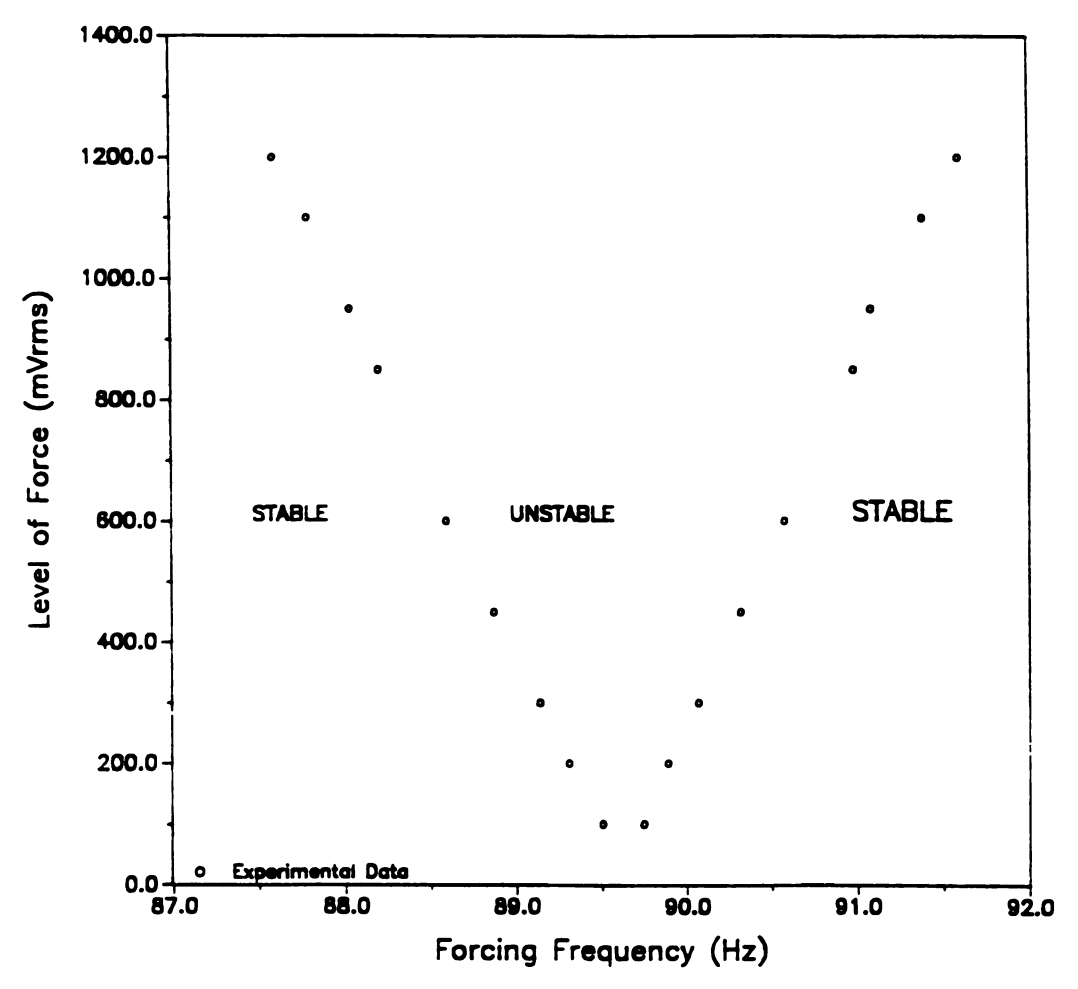


Figure 4.3: Stability diagram for fourth mode.

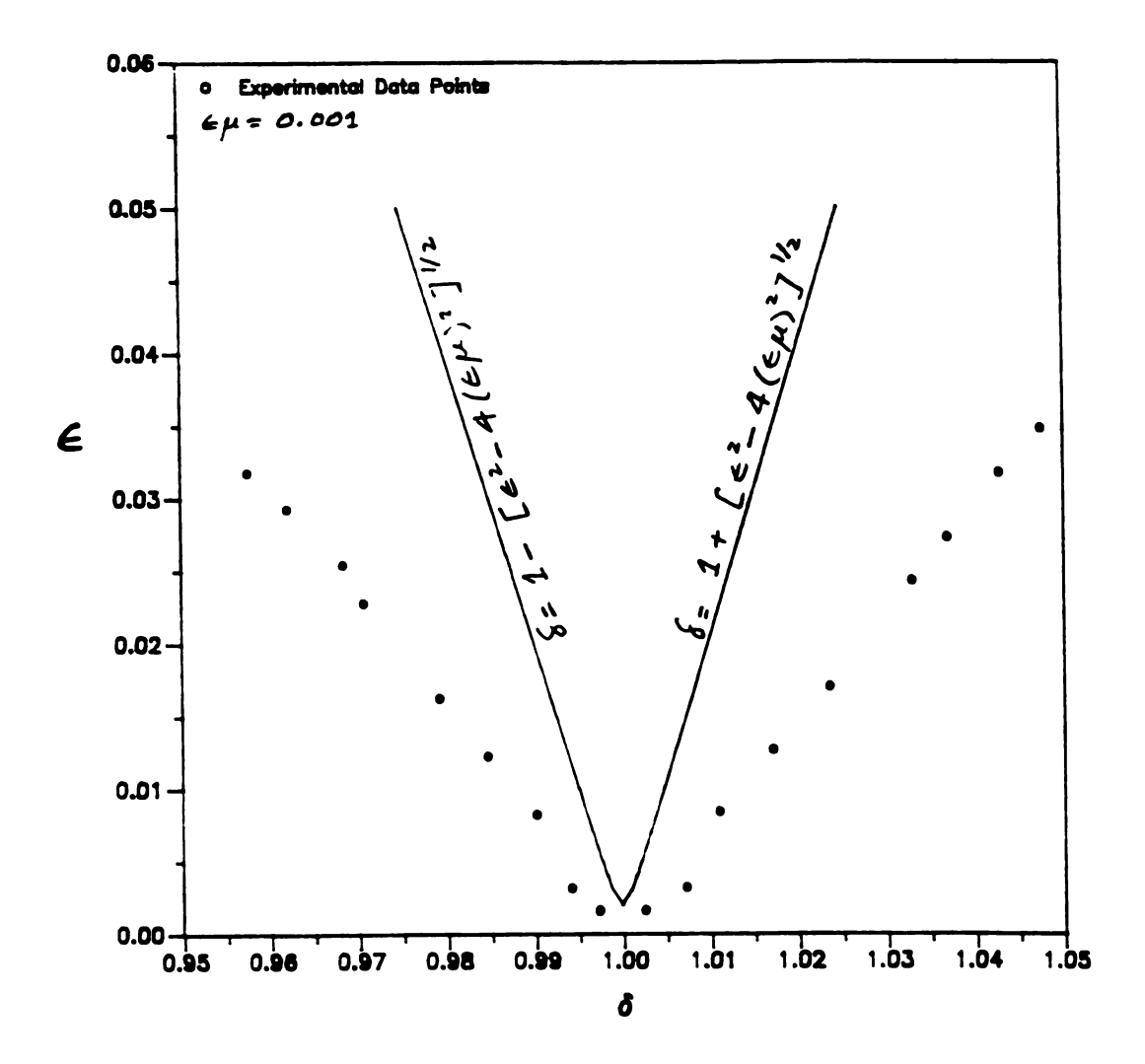


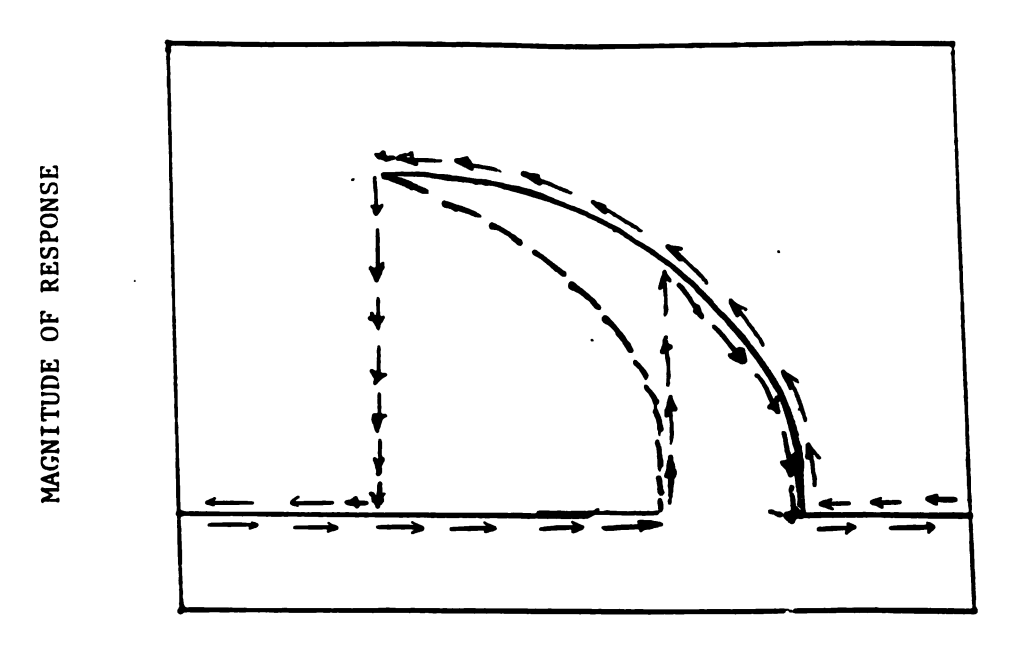
Figure 4.4: Comparision of theoretical Strutt diagram with experimental data points for fourth mode.

response grows the linear theory is no longer valid and the effects of non-linearities cannot be ignored. If the response remains inplane and contains essentially one mode, the motion is governed by the nonlinear Mathieu equation as derived in Chapter 2, equation (2.24) (also see Evan-Iwanowski [1976]). This equation admits nontrivial, steady-state solutions. Approximate solutions to this equation can be found (see, for example, Nayfeh & Mook [1979] pp 169, 338-348) and it can be shown that non-trivial, steady-state solutions exist over a range of forcing frequency. The general form of the variation of the amplitude of the steady-state solutions, as a function of the forcing frequency, is sketched in Figure 4.5a. The experimental results presented in Figure 4.5b substantiate these theoretical predictions. The data for Figure 4.5b was obtained by measuring the amplitude of the response at various values of the forcing frequency. The base acceleration is kept constant at 7.81 m/s² throughout. A typical time trace of the forcing term and the associated response are shown in Figure 4.6 along with their corresponding Fourier transforms. It can be noted that the frequency of the response is one half of the frequency of the excitation. This corresponds to a main parametric resonance.

The frequency response curve of Figure 4.5b shows the possible existence of multiple steady state solutions. At a frequency, say of 89 Hz, two stable steady state solutions can be obtained, one at A (trivial) and the other at B (non-trivial). The response adopted depends on the initial conditions of the system.

4.3 Chaos

If the level of force is increased, corresponding, say, to a base acceleration of 31.44 m/s^2 , then the amplitude response curve presented in Figure 4.7 results. As might be expected, the response amplitudes are larger. However, an interesting additional feature develops. At large amplitudes the response becomes chaotic.



FREQUENCY

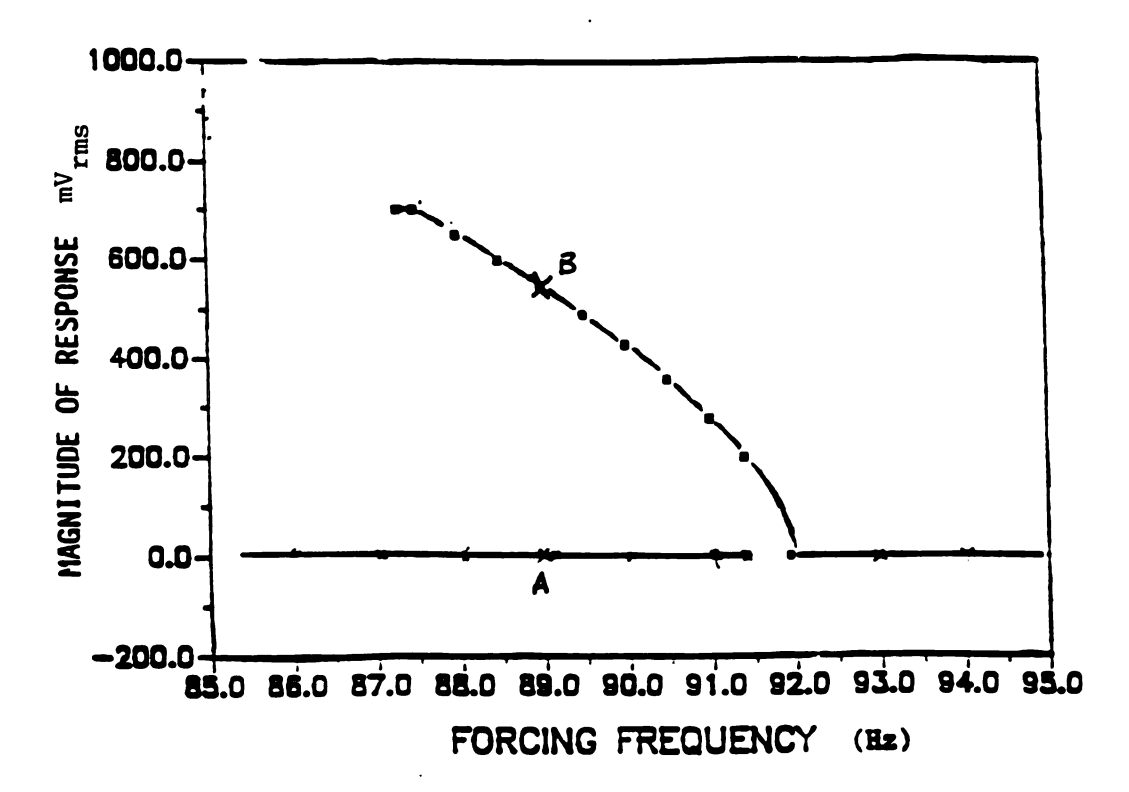
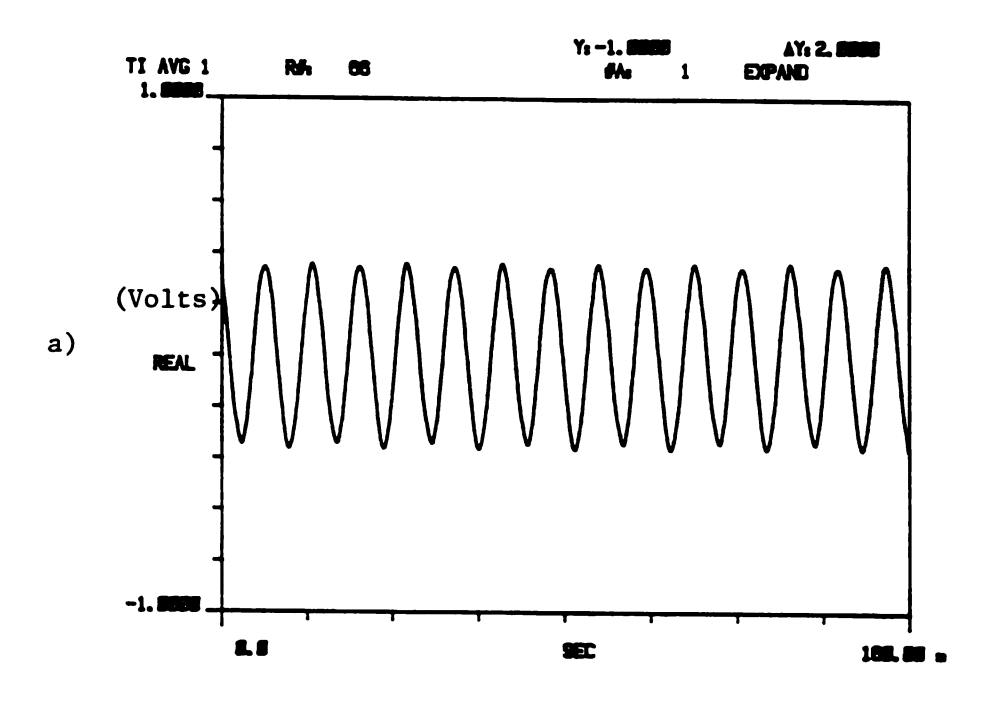


Figure 4.5: a) Sketch of frequency-response curve for nonlinear Mathieu's equation.

b) Experimental frequency-response curve for cantilever beam. Level of force canstant.



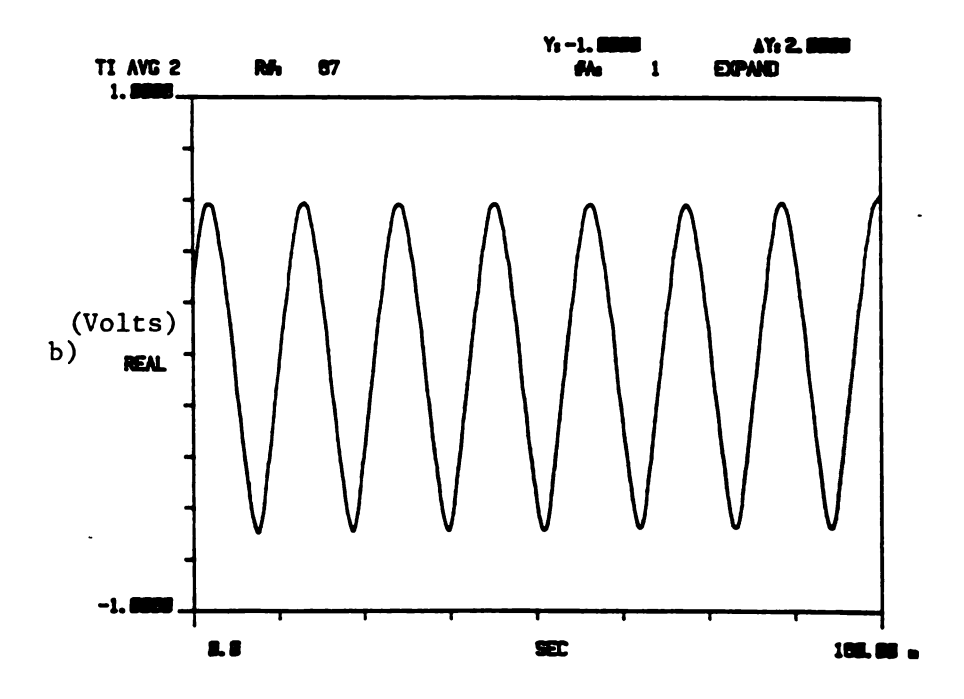
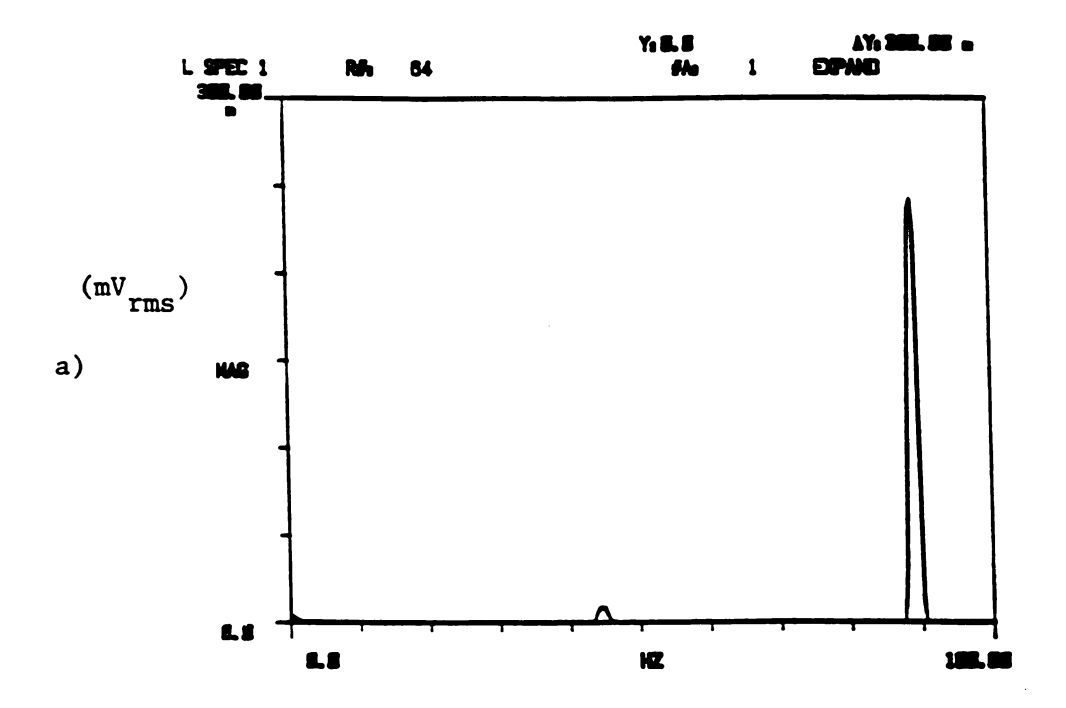
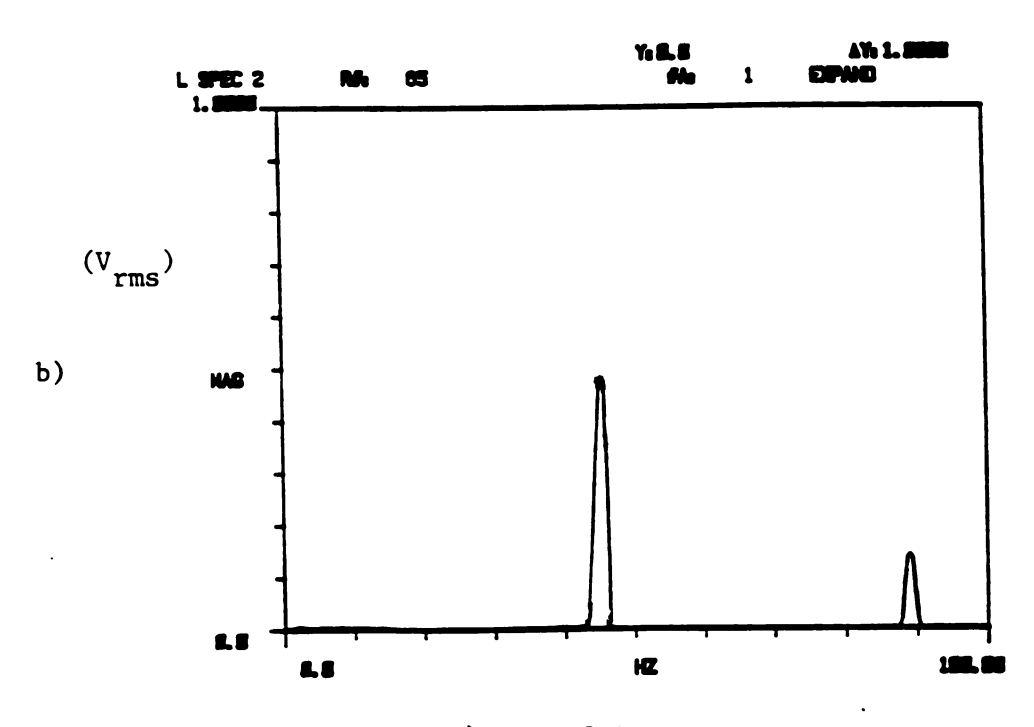


Figure 4.6: Time trace showing a steady-state parametric response.

a) input b) output





a) FFT of input in Figure 4.6

b) FFT of output in Figure 4.6

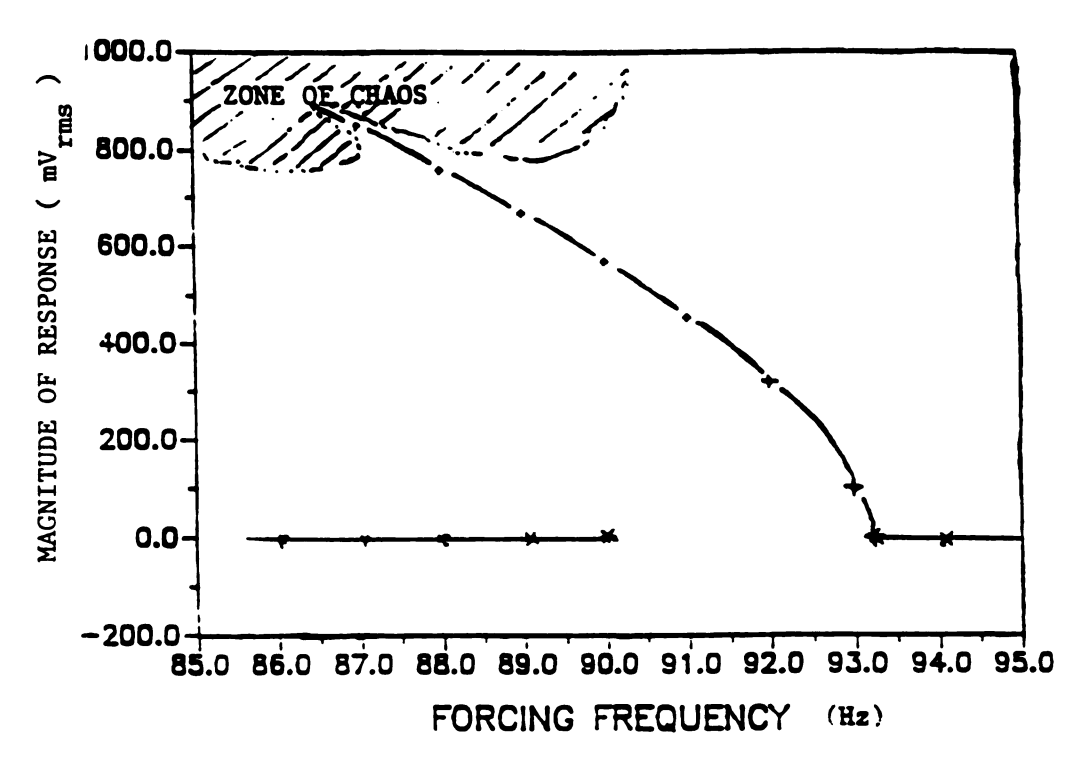


Figure 4.7: Experimental frequency-response curve for cantilever beam. Level of force constant but higher than Figure 4.5b.

The chaotic motions observed for the model are associated with the non-planar response of the cantilever. The particular type of non-planar response observed has, to the best of the author's knowledge, not been reported in the literature. To appreciate the physics of this response, the reader is referred to Figure 4.1 in which the static equilibrium position (s.e.p) of the cantilever is depicted. In this position the stiffness associated with a rotation about the x-axis (torsion) and the stiffness associated with the bending in the x-z plane are very high compared to the bending stiffness in the x-y plane. However, when the beam deflects in the x-y plane, these stiffnesses reduce drastically. An oscillation out of the x-y plane can now occur but can only be sustained while the beam remains away from the s.e.p.. When this out of plane oscillation occurs, the beam gets locked-over on one side of the s.e.p.. It is this out-of-plane motion that is at the heart of the chaos which has been observed. For example, if the phasing of the out of plane motion is just correct, then, as this motion passes through the x-y plane, it is possible for the beam to snap through to the other side of the s.e.p.. Even if this snap through does not occur, the resulting motion is highly sensitive to small perturbations, especially as the beam approaches the s.e.p..

The various kinds of chaotic response observed in and about the "zones of chaos" (see Figure 4.7) are classified as:

- i) Transient Chaos,
- ii) Intermittent and Steady-State Chaos,

The experimental results for these responses are presented and discussed in the following sub-sections.

4.3.1 Transient Chaos

The appearence of chaotic motions for a short period of time, before settling down to steady-state trivial or non-trivial value is termed transient chaos. Such transient chaos appears in the system when the response is quite large, e.g point C on Figure 4.7. It is then possible to observe transient chaos, if the system is perturbed from its steady-state. The transient chaotic response never remains choatic, but always returns to either the trivial or the non-trivial, single mode steady-state value.

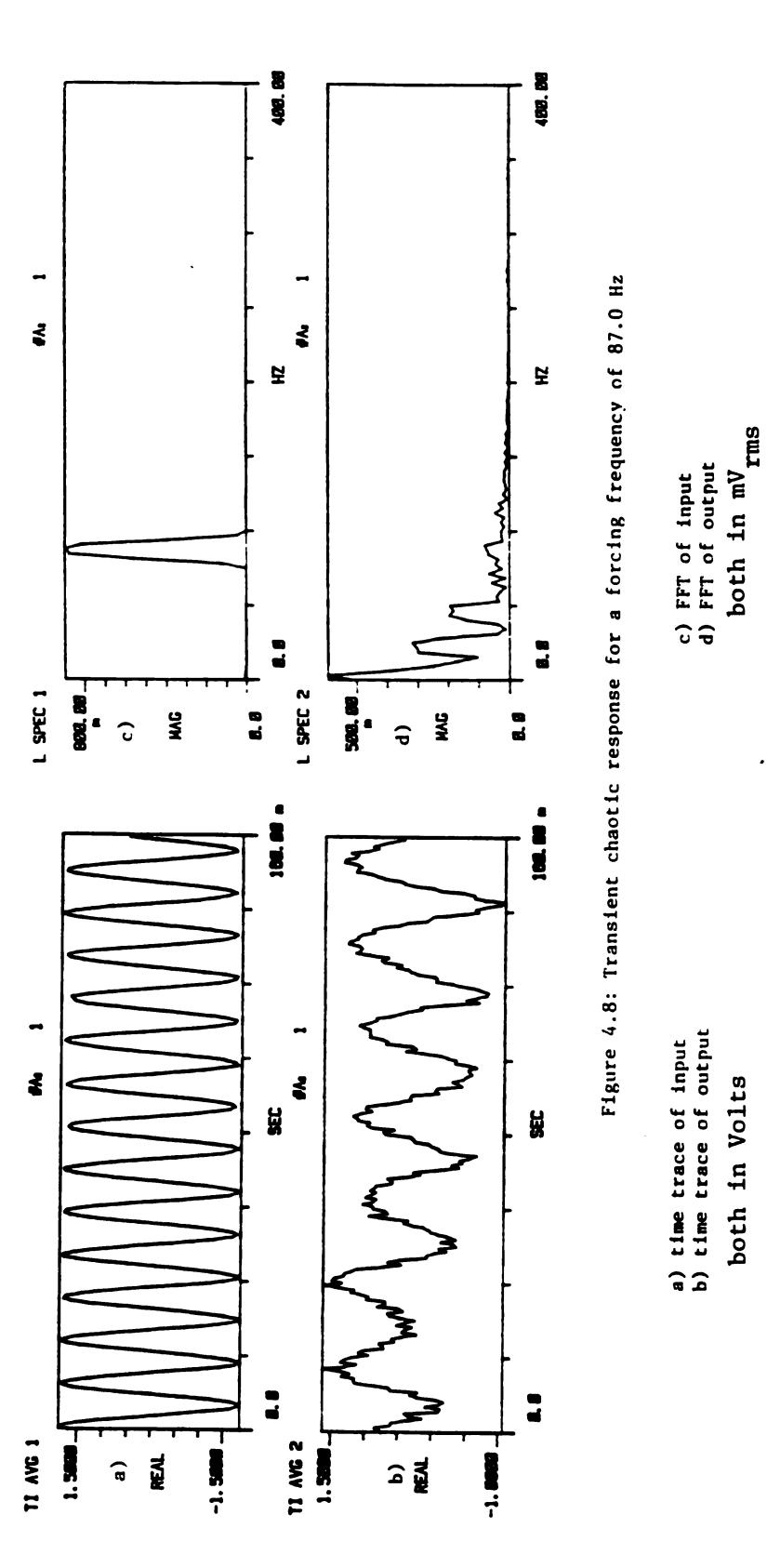
Transient chaos in the beam was observed when the system was perturbed from its steady- state, in-plane, mode 4 motion by gently tapping the model with one's hand. The system was being forced at 87 Hz and level of force was 31.44 m/s^2 . Time traces of the forcing term and the response along with their associated Fourier transforms are shown in Figure 4.8. Note that the Fourier transform of the response shows a broad band power spectra which is typical of a chaotic motion. The transient chaotic motion subsided and the beam returned to single mode 4, in-plane, steady-state motion after approximately 250 cycles of forcing term.

As in all nonlinear phenomena, it is important to allow a long enough period of time to pass before pronouncing that the final form of the response has been reached. A sufficient time to classify chaos as transient or steady state is a matter of judgement of the investigator, but we considered 30,000 cycles of forcing frequency as a sufficient time for pronouncing the chaos as steady state.

4.3.2 Intermittent and Steady-State Chaos

Intermittent chaos is a burst of chaotic motion occurring between periods of regular motion (see Moon [1988] pp 59,181), whereas steady-state chaos refers to the fact that the response remains chaotic for all time even when perturbed more than an infinitesimal amount.

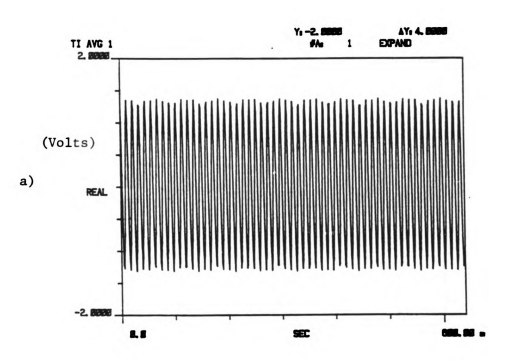
Referring to Figure 4.7, if the frequency is decreased enough, an out of plane mode is excited and a chaotic response results. The physical system's response was observed to cycle back and forth between chaotic and mode 4 motions indicating a transition to chaotic motion via the intermittency route, as reported by Burton



and Kolowith [1988]. The intermittent chaos was observed for a downward sweep of frequency at a constant level of force. It appeared that the time spent in chaotic bursts increased as compared to time spent in periodic motion as the level of force was increased.

Steady-state chaos in this system occurs if the frequency is decreased enough. The system may achieve steady-state chaos with or without going through the intermittency route. However, if intermittent chaos is present, an increase in the level of force results in steady state chaos. An example of such a steady state chaotic response is shown in Figure 4.9. The cantilever was being forced at 87.1 Hz and the level of the force corresponds to 40 m/s^2 . The system was responding in a single, mode 4 motion prior to the onset of the chaos. The chaotic response shown is very complex in the sense that although only a few modes are present, they come and go in a chaotic manner. The Fourier transform of the response presented in Fig. 4.9 suggests that the 2nd, 3rd, and 4th, in-plane (x-y plane) vibration modes are involved in the chaotic motion. A similar observation was made by Burton and Kolowith [1988].

An example of the system attaining steady-state chaos without going through the intermittent chaotic stage was observed while the system was responding in the third transverse in-plane mode. The cantilever was forced at a frequency of 45 Hz. The time traces shown in Figure 4.10 show the cantilever's response for the third mode in plane transverse vibration. When the frequency was decreased to 43 Hz while keeping the level of force constant, the cantilever jumped into chaotic motion without going through intermittent chaos. The time trace along with its Fourier transform of this response are shown in Figure 4.11. Clearly, the response has developed into a very complex form. Even when perturbed a little it remains in this state for all time.



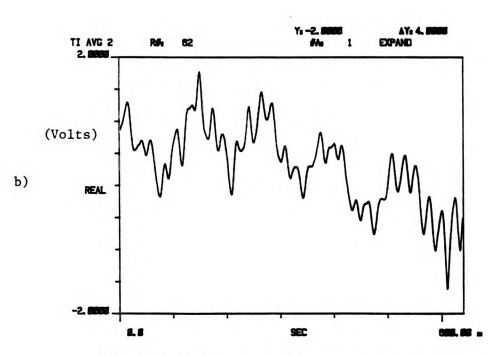
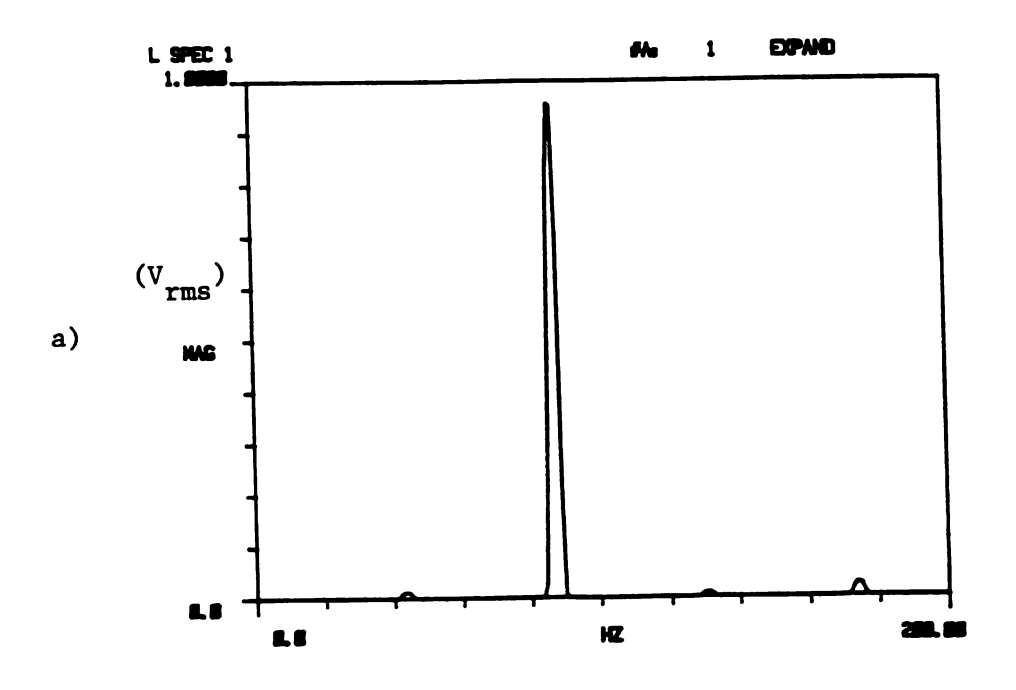
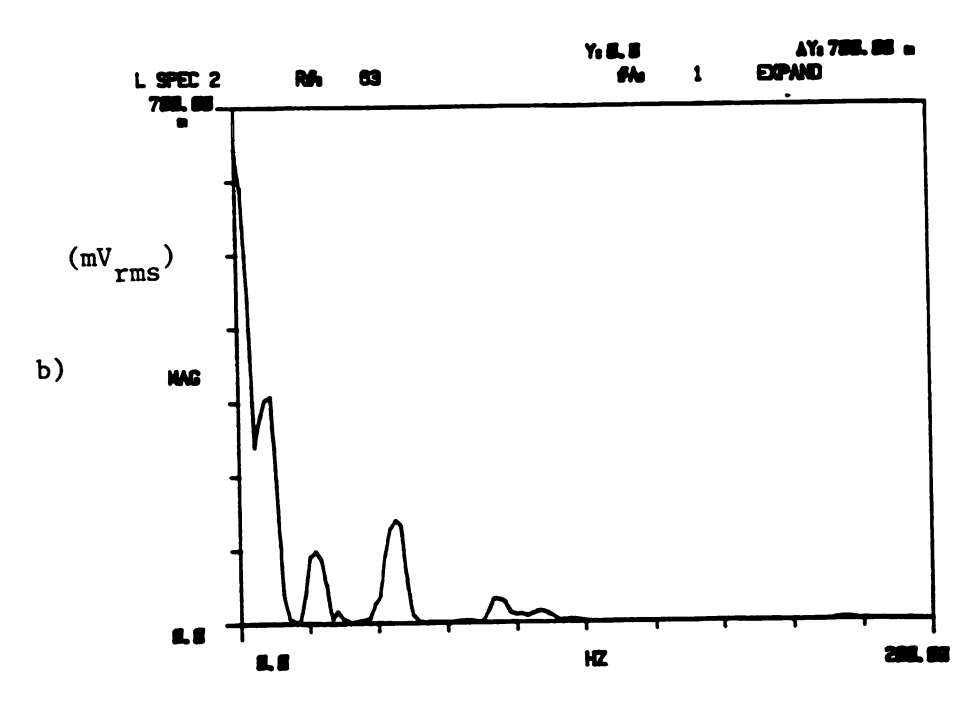


Figure 4.9: Robust . chaotic response for a forcing frequency of 87.0 Hz.

a) input b) output





a) FFT of input in Figure 4.9

b) FFT of output in Figure 4.9

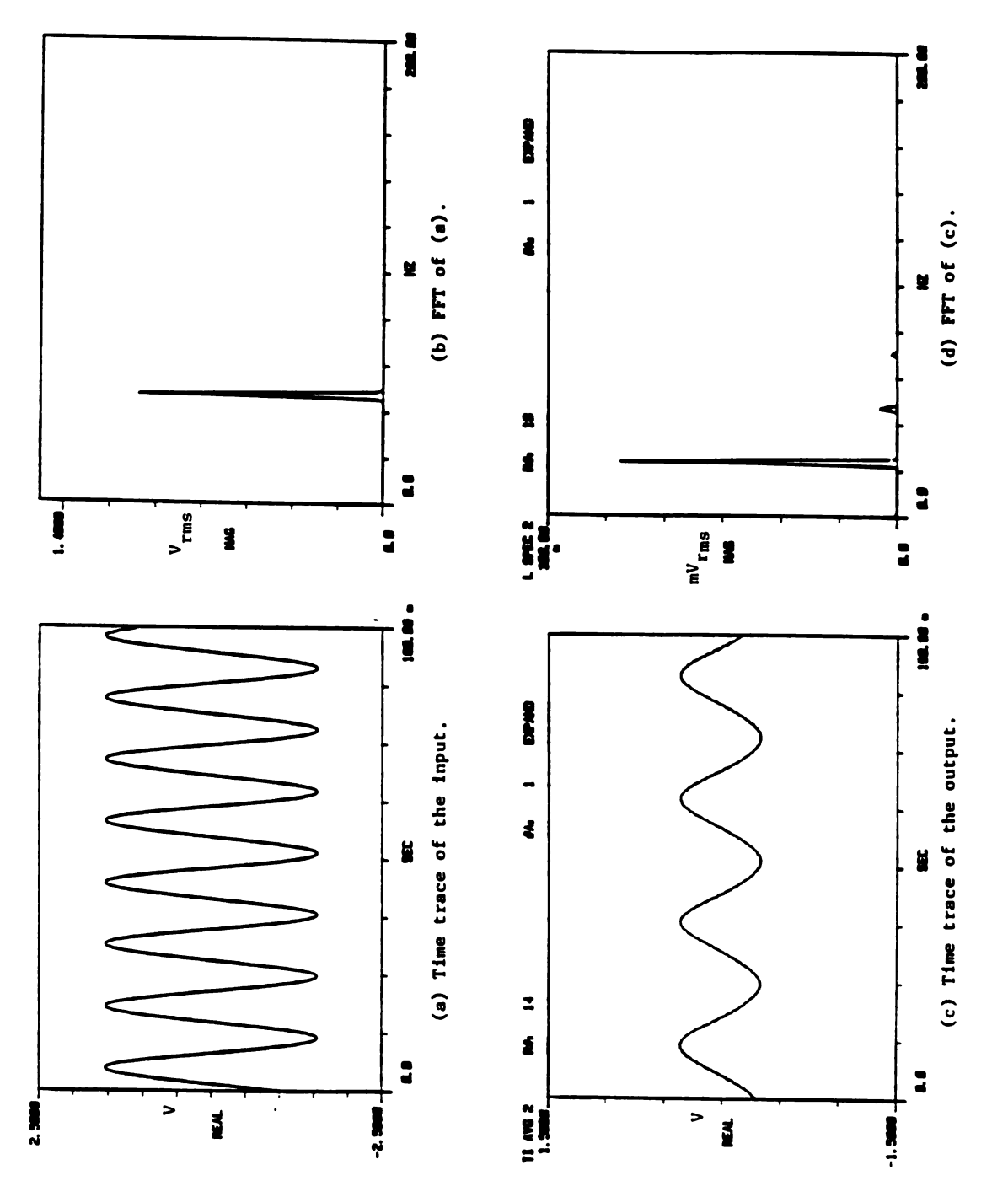
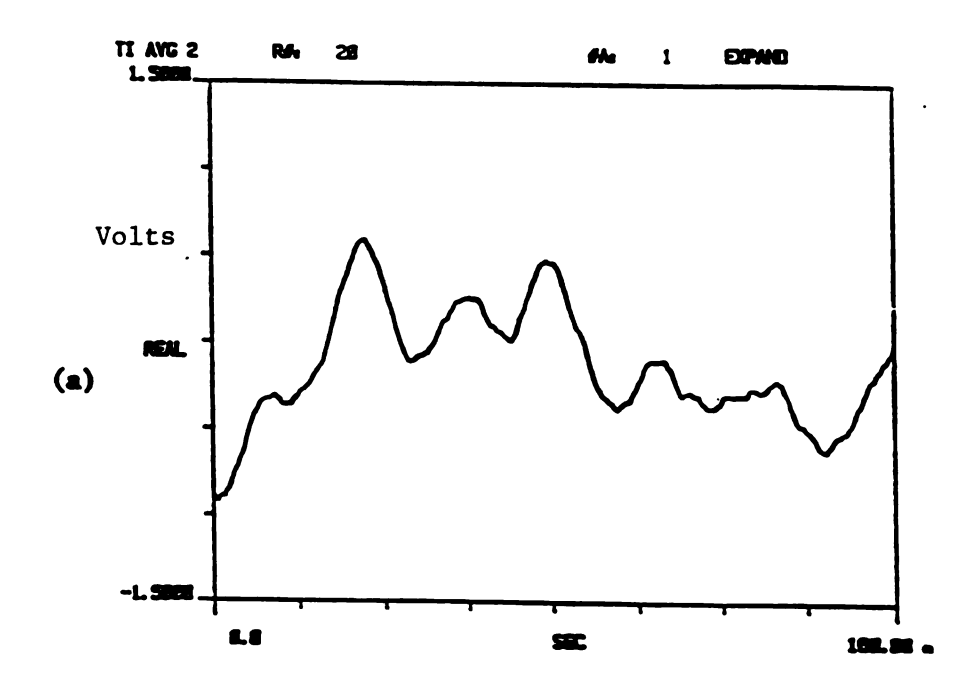


Figure 4.10: . Steady-state time traces showing parametric response for a forcing frequency of 45 Hz.



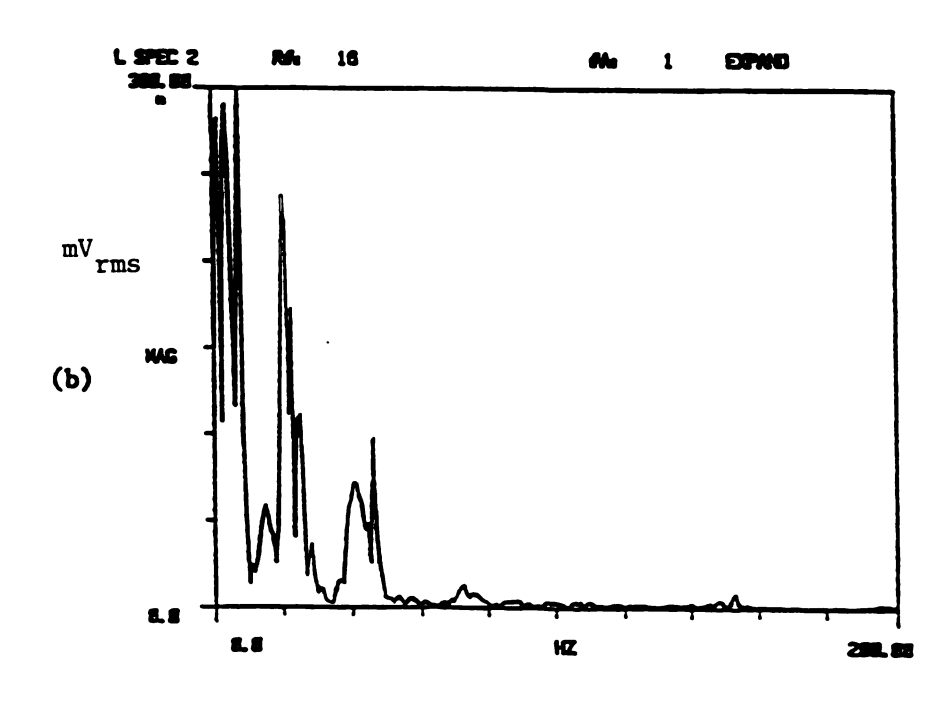


Figure 4.11: Chaotic response for a forcing frequency of 43 Hz.

- a) FFT of output
- b) output

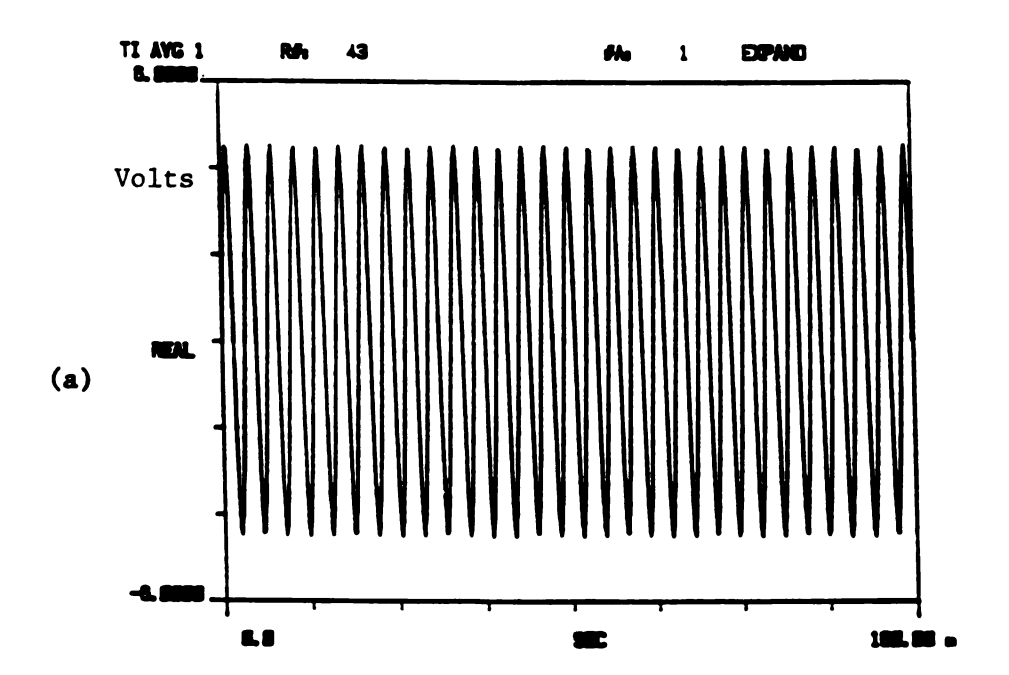
4.4 Multi-Mode Interaction

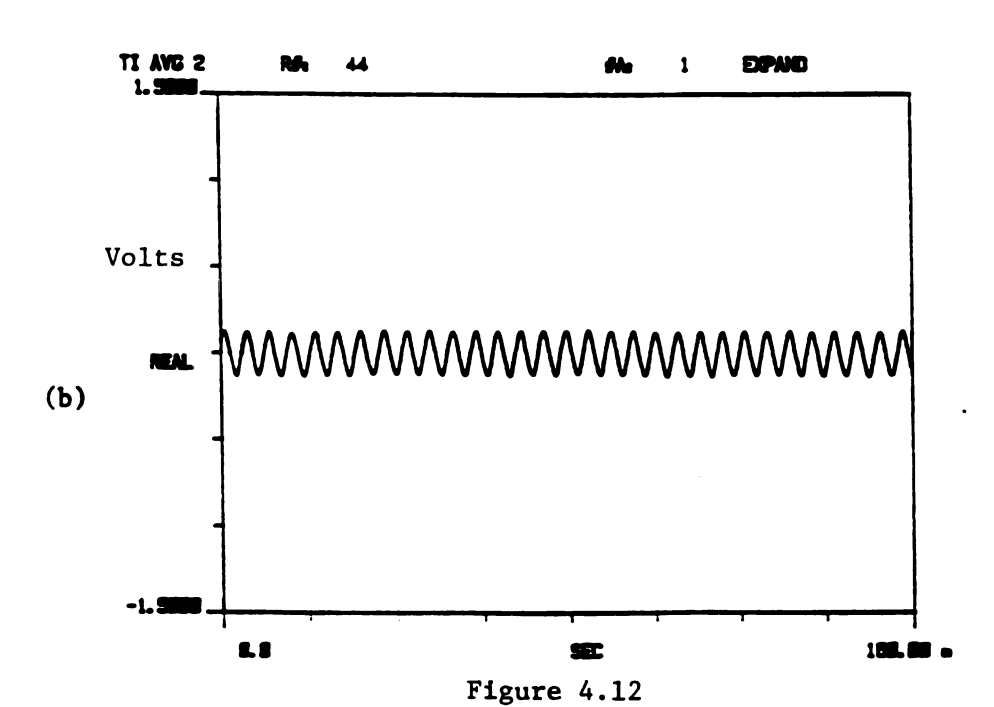
Internal resonance, i.e when the natural frequencies of a system are commensurable, can greatly enhance the coupling between modes. Haddow et al. [1984] showed experimentally and theoretically the effect of internal resonance on a two degree-of-freedom system. Barr [1980] described the possibility of a "cascading" of energy through the modes of a multi-degree-of-freedom system as a result of internal resonances. It is believed that such a "cascading" is occurring in this experimental model when a high frequency input gives rise to a low frequency, high amplitude response. Experimental results showing the existence of this phenomenon are presented and discussed in the sub-sections to follow.

4.4.1 Extremely Low Subharmonic Response

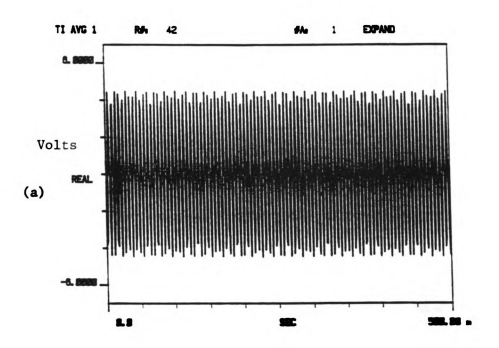
Although Dugundji and Mukhopadhyay [1973] reported on the theoretical possibility of exciting a low frequency mode in an axially excited thin beam, no experimental results have been reported in the literature. Such a response was observed in our physical system.

Figure 4.12 shows a time trace of the input and the output for an initial time close to zero. This is for a forcing frequency of 190 Hz. Figure 4.13 again shows the input and output some 30 seconds later. Note that the scales have been changed in order to better show the form of the response. It should be stressed that the forcing function remains the same in Figures 4.12 and 4.13. Over the 30 seconds, a high order sub-harmonic with a period about 40 times higher than the forcing term has developed (see Figure 4.14 which shows Fourier transforms of Figure 4.13). Moreover, there has been an extremely large increase in the amptitude of the response. This is a consequence of the energy input being transformed from a small amplitude at a higher frequency to a large amplitude at a very low frequency.





Initial time traces of the (a) input, (b) output.



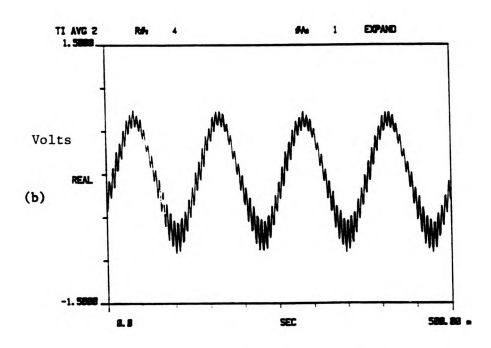
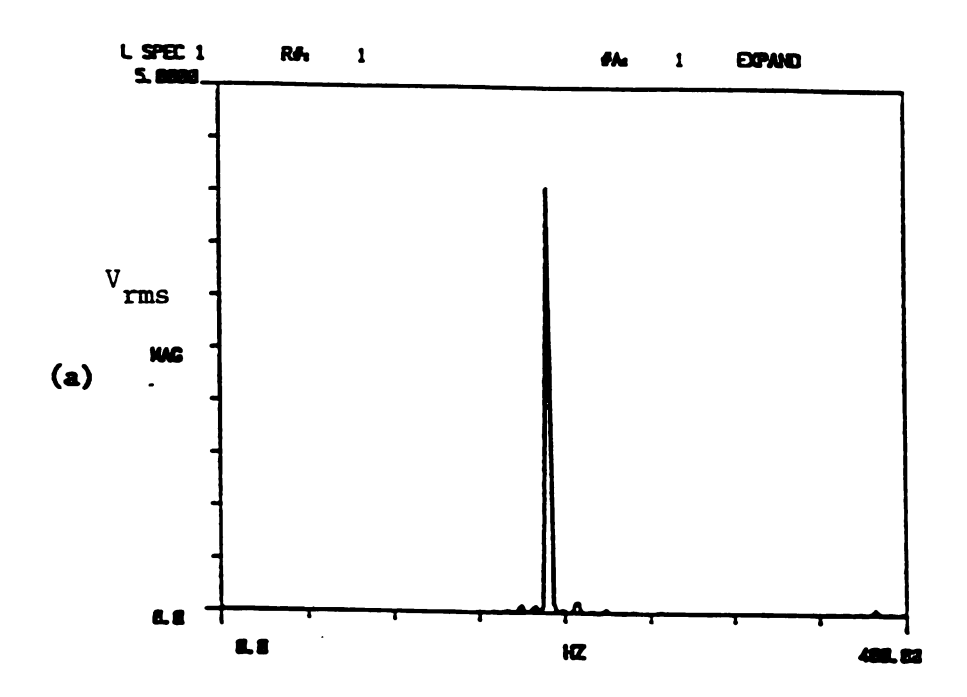


Figure 4.13: Traces at time +30 secs. (a) Time trace of the input (the variation in the amplitude is a consequence of the digitizing).

(b) Time trace of the output.



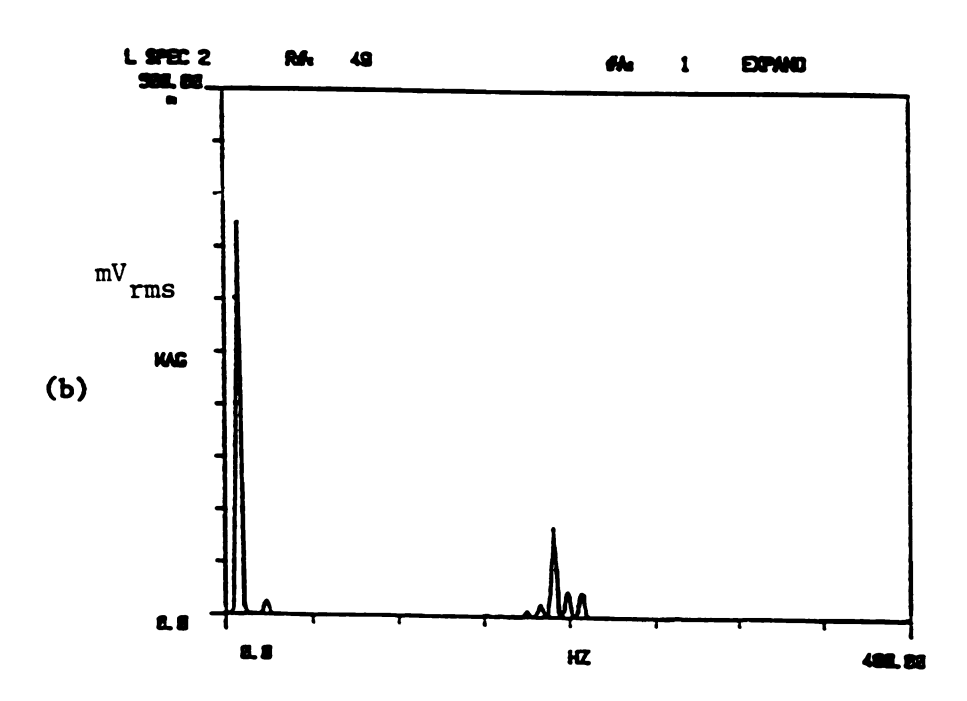


Figure 4.]4: FFT of time trace t+30 secs

- a) inputb) output

4.4.2 Modal Interaction and Beating Phenomenon

Another class of interesting response has been observed. It results from a combination resonance which in turn excites a regular parametric response. Figure 4.15 shows the waterfall plot of the frequency content of this interaction for an initial time close to zero. The waterfall plot gives the variation of the frequency content of a time signal as a function of time. The system was forced at a frequency of 385.60 Hz, which is close to 12th linear transverse natural frequency. In this case, the response frequency was the same as the forcing frequency. Such a response is consistent with a secondary parametric instability.

The forcing frequency acts as a parametric excitation term for the combination resonance case of $\Omega_f \approx \Omega_4 + \Omega_{12}$, where $\Omega_4 = 44.8~Hz$ and $\Omega_{12} = 337.5~Hz$ are the 4th and 12th linear transverse natural frequencies respectively. We believe that the nonlinearity adjusts the frequencies of the 4th and 12th mode so that the resonant frequency combination is satisfied. This results in exciting the 4th and 12th linear mode of the system, and we see the model responding at 45 Hz and 337.5 Hz, simultaneously, after approximately 350 cycles of forcing frequency. See Figure 4.15. After 2200 cycles of the forcing frequency, another regular main parametric response is generated at 22.5 Hz. This occurs because the response at 45 Hz acts as a parametric excitation on the third linear mode (i.e $\Omega_3 = 22.5~Hz$). Thus the response is now a combination of several modes and the model is responding simultaneously at frequencies of 22.5 Hz, 45 Hz, 337.5 Hz and 385.6 Hz.

Figure 4.16 shows the waterfall plot of the response discussed above some 10 seconds later (i.e some 3,850 cycles of the forcing frequency). The forcing frequency is the same. Note that the third and fourth modes have not attained steady-state. Instead, there is a continual exchange of energy between these modes. This is an example of a beating phenomenon. Another response is generated at 409 Hz which is not accounted for. This response appears after response

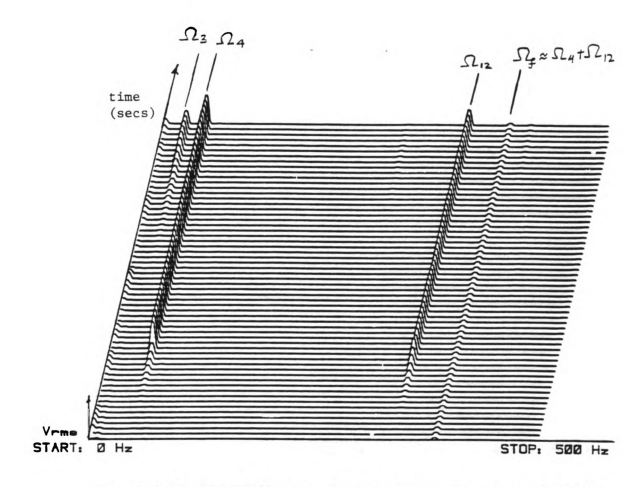


Figure 4.15: Waterfall plot showing output close to an initial time zero for a forcing frequency of 385.6 Hz.

 $\Omega_3 = 22.5 \text{ Hz}$ $\Omega_4 = 45.0 \text{ Hz}$ $\Omega_{12} = 337.5 \text{ Hz}$ $\Omega_f = 385.6 \text{ Hz}$

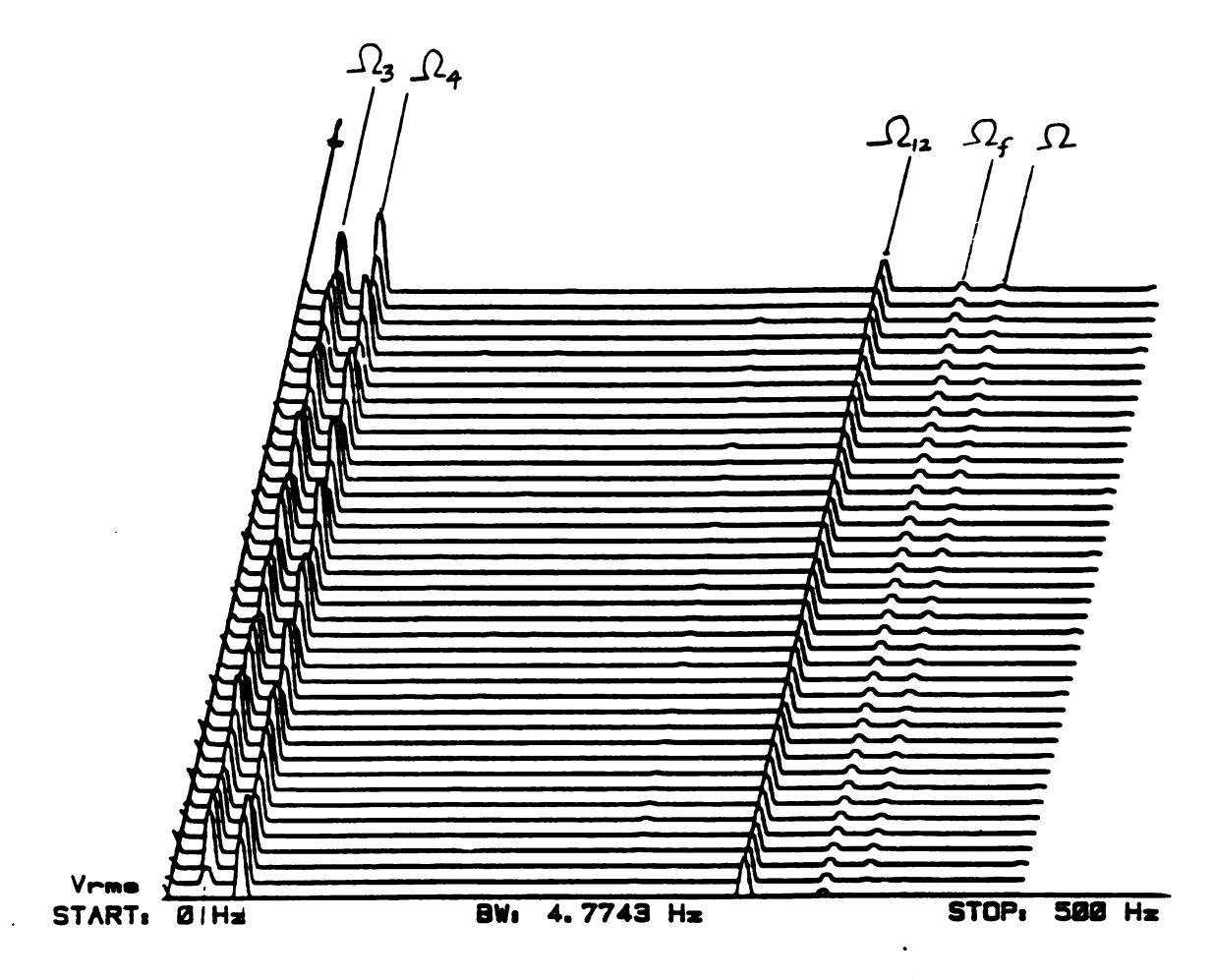


Figure 4.16: Waterfall plot showing output some t+10 secs later for a forcing frequency of 385.6 Hz.

 $\Omega_3 = 22.5 \text{ Hz}$ $\Omega_4 = 45.0 \text{ Hz}$ $\Omega_{12} = 337.5 \text{ Hz}$ $\Omega_f = 385.6 \text{ Hz}$ $\Omega = 409 \text{ Hz}$

at 22.5 Hz is generated and the system starts exhibiting beating phenomenon.

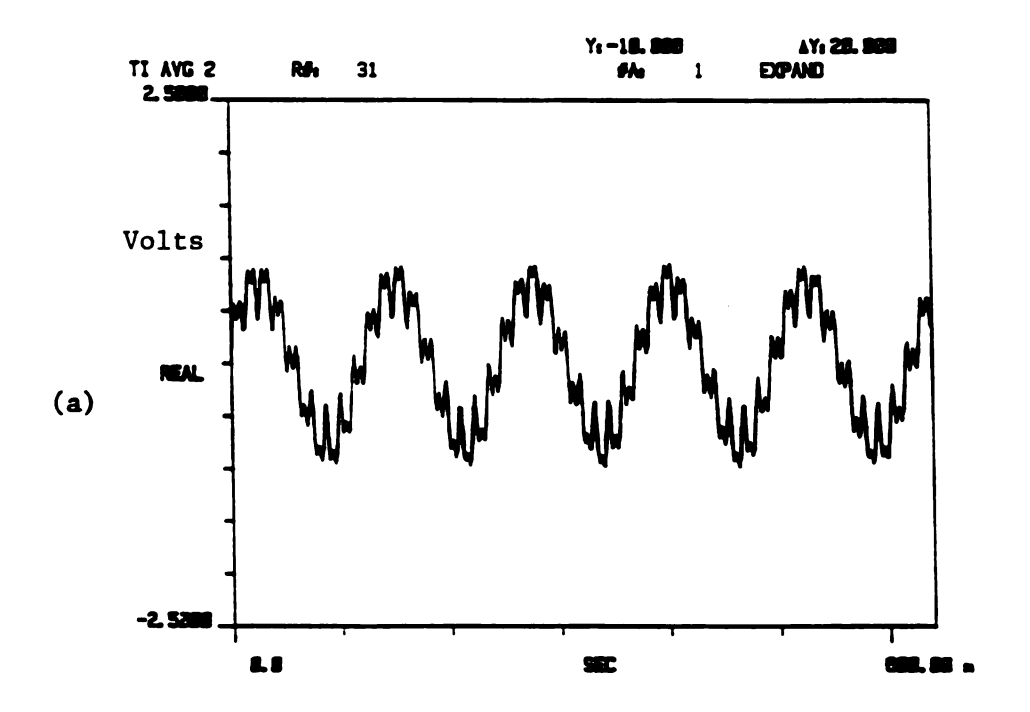
Both the waterfall plots presented in Figures 4.15 and 4.16 span an interval of time corresponding to approximately 3500 cycles and 2400 cycles of forcing term respectively. The form of the response shown in Figure 4.17 remained unchanged even after some 30,000 cycles of the forcing term.

The response presented above is a consequence of internal resonance. It is important to note that a high frequency, low amplitude input, eventually leads to a large amplitude response which is at a very low frequency.

4.4.3 Combination Resonance

An interesting observation regarding a combination resonance was made while the physical system was in a chaotic regime born from a fourth mode oscillation. If the system was preturbed in a suitable manner, the chaos disappeared and the solution becomes periodic. The response was observed to be a combination of several modes. A time trace depicting this motion is presented in Figure 4.17 along with its Fourier transform. The system was being forced at a frequency of 85.5 Hz with a base excitation of $40 \ m/s^2$. Figure 4.18 shows the response before the combination resonance was attained.

It was interesting to note that this combination could not be attained by starting from the trivial solution. Presumably, the domain of attraction of the combination resonance was very small and, perhaps coincidently, the chaotic motion passed closed to it. However, its response was relatively robust in the sense that once the combination resonance had been attained, it was insensitive to perturbations.



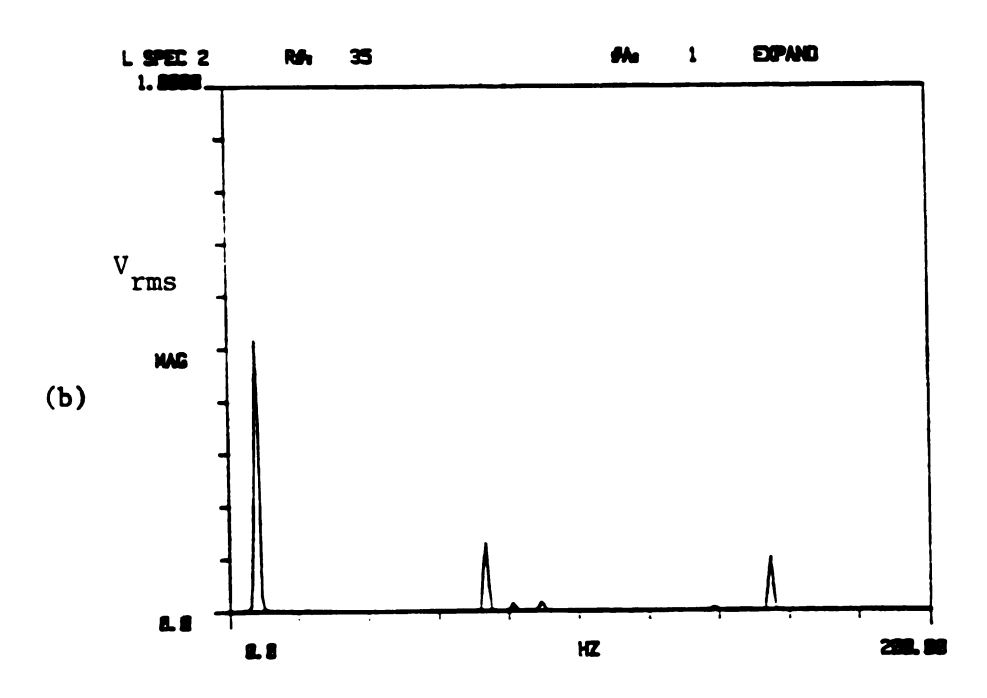
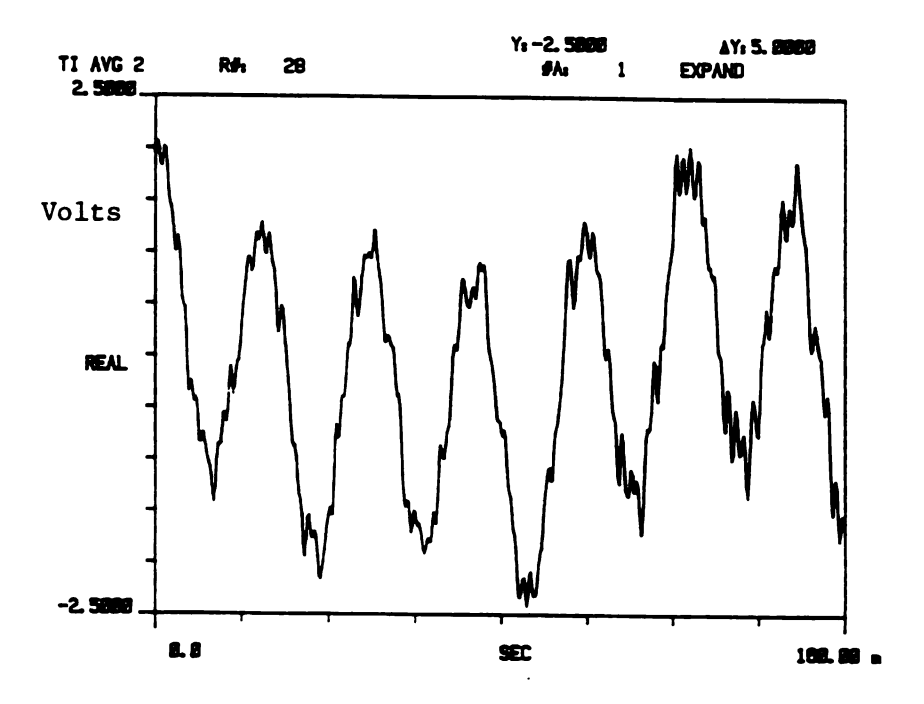


FIGURE 4.17 Combination of responses at a forcing frequency of 85.5 Hz. (a) Time trace of the output.

(b) FFT of (a).



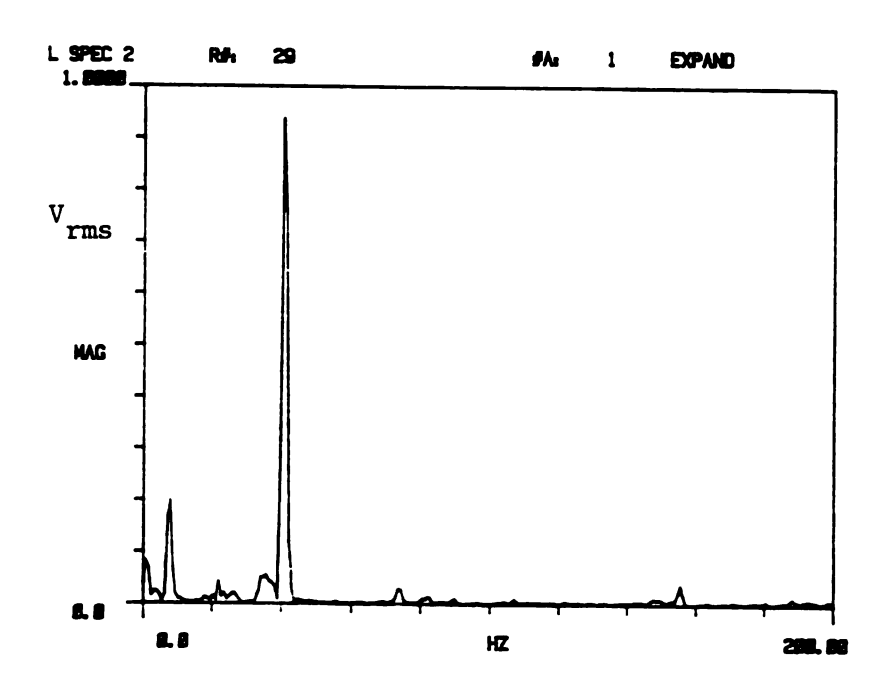


Figure 4.18: Chaotic response for a forcing frequency of 85.5 Hz.

- a) timetrace of outputb) FFT of output

CHAPTER 5

DIMENSION ESTIMATE

5.1 Introduction

For continous systems the number of modes necessary for a full dynamical description becomes large, and in theory sometimes infinite. From a practical standpoint one must truncate this model to just a few mode shapes, i.e those modes which contain the most information about the 'true' system dynamics. Most often modal truncations are based upon retaining only the most energetic mode shapes.

Since chaotic systems produce power spectra with many peaks, or even of continuous form, it is often unclear how many modes should be retained. The Hausdorff dimension D (see Burge et.al [1984] pp 146), is defined as

$$D = \lim_{\epsilon \to 0} \ln \frac{N(\epsilon)}{\ln \frac{1}{\epsilon}}$$
 (5.1)

where $N(\epsilon)$ is the smallest number of hyperecubes necessary to cover the attractor (see Guckenheimer and Holmes [1986] pp 256-257). This can be regarded as the average number of linearly independent coordinates necessary to describe a dissipative dynamical system. Thus the Hausdorff dimension gives the modeller a tool by which to approximate the number of active modes in a system.

However, the Hausdorff dimension has the following drawbacks:

- i) The computation is very time consuming since it converges slowly when the dimension of the phase space is greater than two (see Burge et al. [1984] pp 149).
- ii) It is a geometric measure. It does not account for the frequency with which the orbit might visit the covering cube (see Moon [1987] pp 214).

Therfore, we must use an alternative way of estimating the dimension of a dynamical system. Some of these which can be used are (see Moon [1987] pp 214):

i) Pointwise dimension as discussed by Farmer et al. [1983] and defined as

$$d = \lim_{n_d \to \infty} \lim_{r \to 0} \frac{\log \frac{1}{n_d} N_{\overrightarrow{x_0}}(r)}{\log r}$$
 (5.2)

where n_d is the total number of data points, and it consists of counting the number of data points $N_{\overline{z_0}}(r)$ within a hyper-sphere of radius r, centered at a point $\overline{z_0}$ on the attractor.

ii) Correlation dimension C(r) as described by Grassberger and Procaccia [1983b] and estimated by

$$C(r) = \lim_{\substack{n_d \to \infty \\ n_r}} \frac{1}{n_r} \sum_{i=1}^{n_r} \frac{1}{n_d} \sum_{i=1}^{n_d} \theta(r - |\vec{x_i} - \vec{x_j}|)$$
 (5.3)

where n_r is the number of reference points, $\vec{x_j}$ are the reference points (vectors), $\vec{x_i}$ are the rest of the points on the attractor, n_d is the number of data points, and θ equals 1 when its argument is positive, and 0 when its argument is negative.

In this work the dimension of the chaotic motion of the cantilever beam is computed using the procedure and computer programs as described by Klewicki et al. [1988]. Pointwise dimension is used to estimate the dimension of the system, since Holzfuss and Meyer-Kress [1985] showed it to be more accurate than the correlation dimension estimate used by Grassberger and Procaccia [1983b]. Before discussing this, the concept of coordinate reconstruction will be introduced.

Often, one cannot measure all of the variables (coordinates) necessary to describe (embed) the phase trajectories of a given system. It is for this reason that techniques of phase portrait reconstruction from a single measured variable have been developed. The basic idea behind phase portrait reconstruction is that

any N-dimensional system can be described, at any instant, by the measurement of N independent variables pertinent to that system. Implicit in the following method is that, at least indirectly, any measured variable (assuming the resolution of the probe is adequate) contains all of the information about the dynamics as prescribed by the equations of motion. Thus the method involves constructing independent coordinates from a single time series.

There are two known methods by which independent coordinates may be constructed from a single time series. These methods were developed concurrently in a heuristic manner by Packard et al. [1980], and formally by Takens [1981]. Takens proved that for a N-dimensional dynamical system, one may be assured to embed its attractor with at most 2N+1 reconstructed coordinates of the form;

$$\overrightarrow{X_n}(t) = [X(t), X(t-\tau), \dots, X(t-n\tau)]$$

or

$$\vec{X_n}(t) = [X(t), X(t), \dots, \frac{d^{n-1}(X)}{dt^{n-1}}]$$

where X(t) is the experimentally measured time series, and τ is a time delay. That is the reconstructed coordinates may be created either by time delaying or differentiating the measured variable. Due to constraints such as the order of the system, and problems with higher order differentiation of the experimental data, the time delay method is usually preferred. In this work, the time delay method is used to compute the dimension estimate.

The computation of a dimension estimate using measurement from only one location on the cantilever beam involves four basic steps, i.e

- i) acquisition of data,
- ii) estimation of the optimal time delay τ ,
- iii) phase coordinate reconstruction using the optimal time delay,

and

iv) computation of the dimesion estimate.

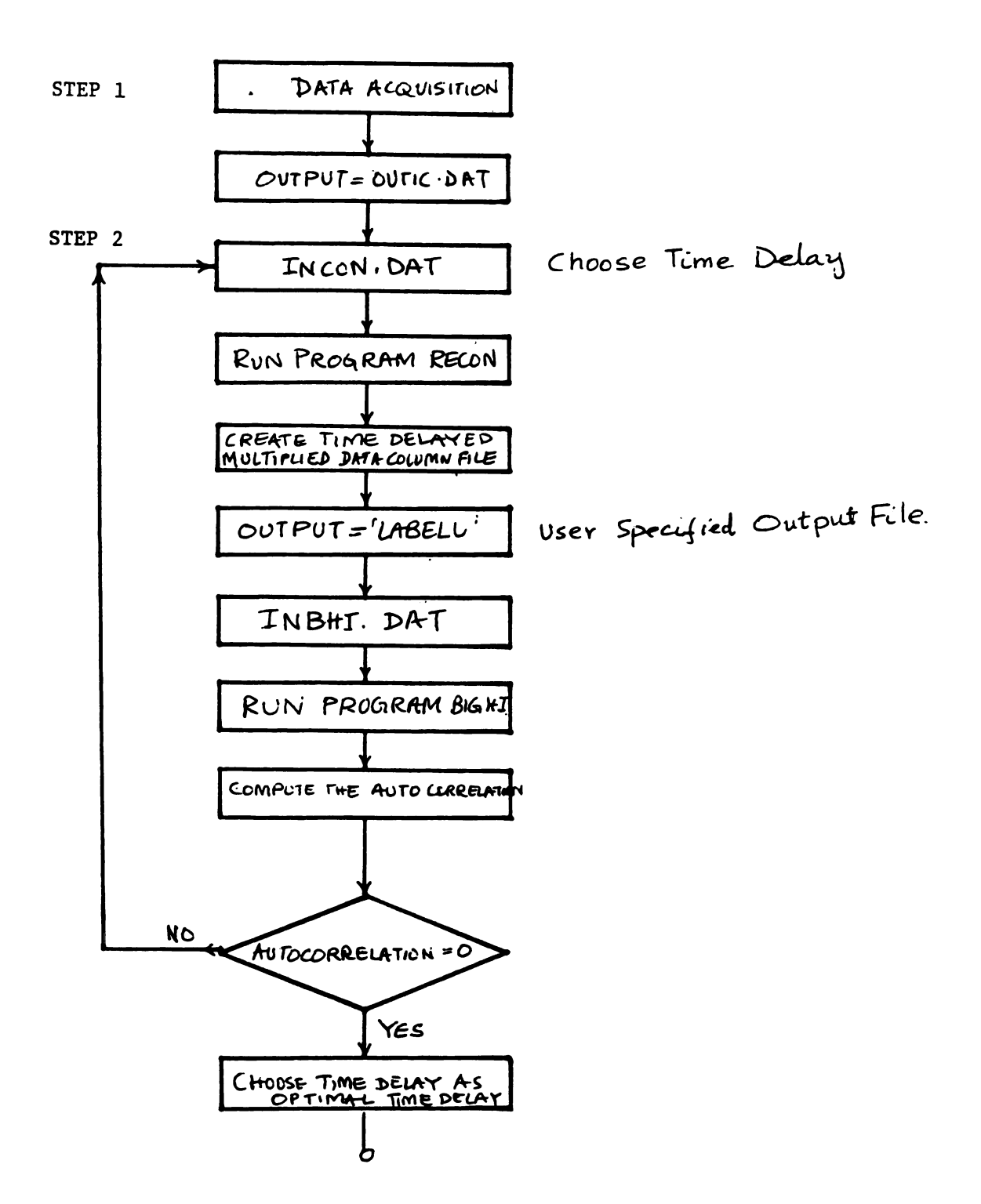
These four steps, as they pertain to the computer programs used, are outlined in the flow chart of Figure 5.1. For more details the reader is referred to Klewicki et al. [1988].

5.2 Acquisition of Data

The data used for dimensional analysis was collected from a chaotic motion arising from the cantilever's third mode motion. The base excitation frequency was 45.0 Hz, and a sampling rate of 1000.0 Hz was used. Record lengths of 40,000 samples were used.

5.3 Estimation of Optimal Time Delay

The process of choosing the time delay used in the phase coordinate reconstruction procedure is subjective (see Klewicki et al. [1988]). Figure 5.2 presents the unnormalized autocorrelation of the data collected from the cantilever beam for various time delays. The curve exhibits a sharp decrease in the first 25 elements (0.025 seconds), then there is a sharp increase for the next 25 elements (intermediate points have been calculated, but not plotted, to check that this trend is correct). The first zero-crossing is at approximately 150 elements. Contrary to the use of the first zero crossing as the criteria for the optimal time delay, (see Klewicki et al. [1988]), the optimal time delay is chosen to be 0.025 seconds. This choice of time delay corresponds to the fact that data has almost lost all information about its past, as evident by the sharp decrease of the autocorrelation function. Notice that the value of optimal time delay chosen is very small.



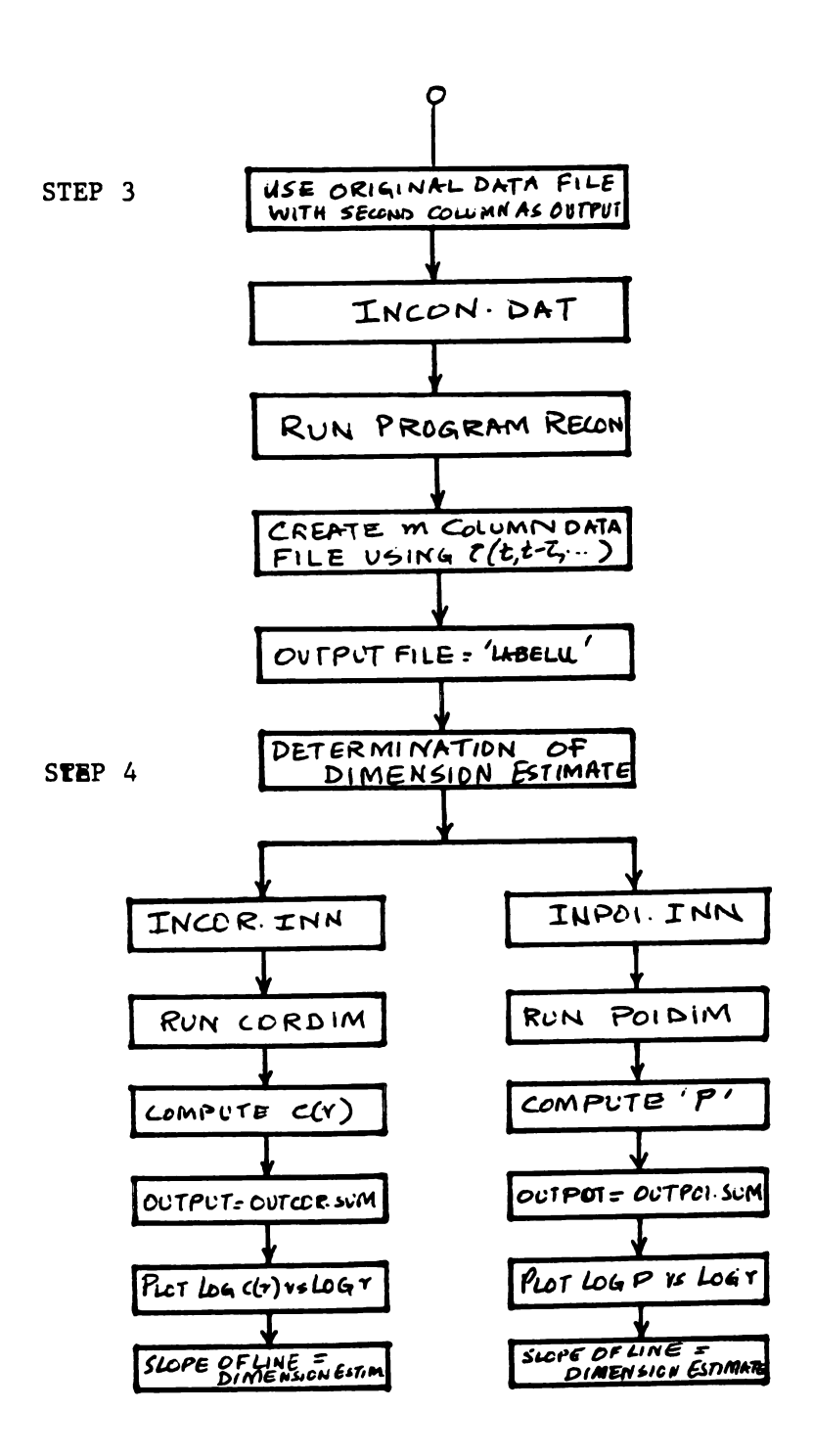


Figure 5.1: Flow chart for the estimation of dimension

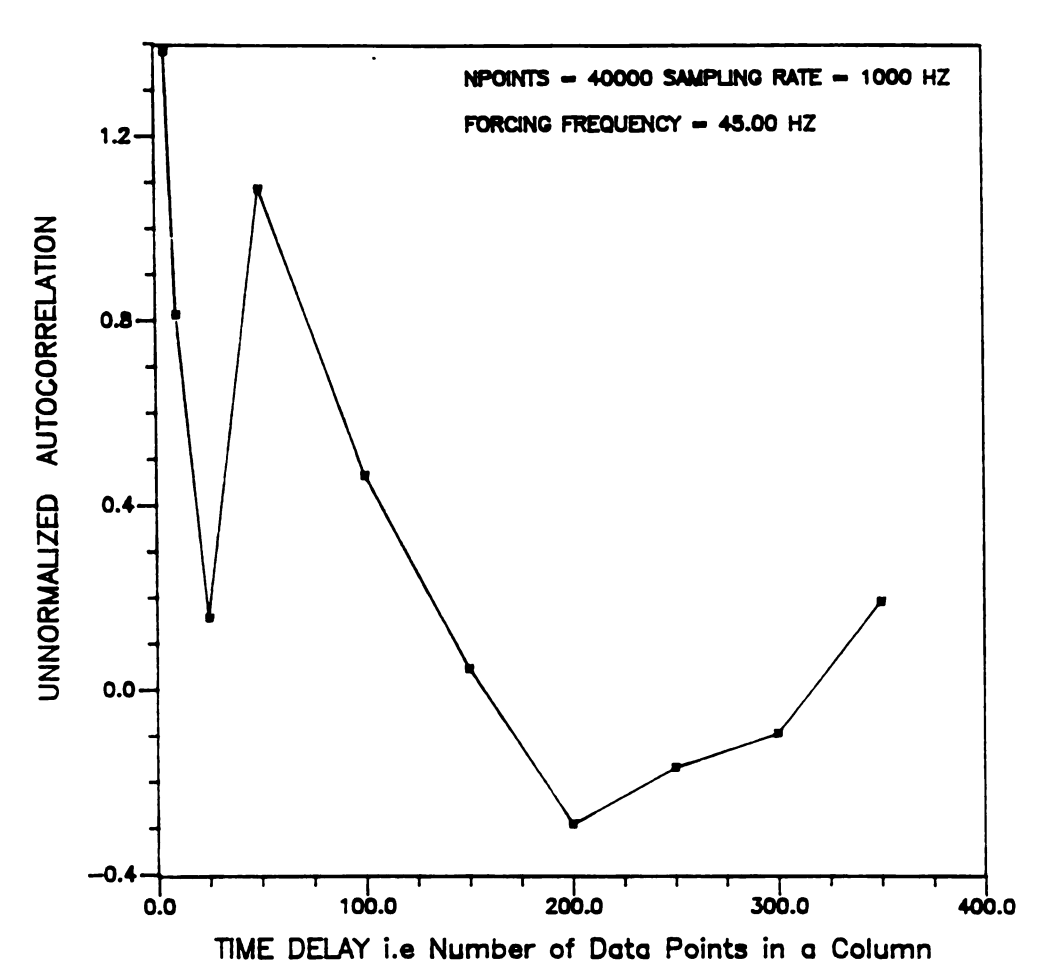


Figure 5.2 The unnormalized autocorrelation function for various time delays.

5.4 Reconstructed Coordinates and Dimension Estimate

The following variables will be used in this section:

N = number of linearly independent coordinates necessary for a full dynamical description of a system,

d = pointwise dimension,

M =integer part of the pointwise dimension,

m = number of reconstructed coordinates used.

To determine the minimum N we calculate a series of pointwise dimensions, d_m , using an increasing number of reconstructed coordinates, m=1,2,3... As m increases, the pointwise dimension, reaches an asymptote, say $d=M+\mu$, where $\mu<1$. Then the minimum number of linearly indepedent coordinates necessary for a full dynamical description for this system is N=M+1 (see Moon [1987] pp 232).

As discussed in the Section 5.3, we have chosen a time delay of 0.025 seconds to reconstruct the coordinates. Figures 5.3a and 5.3b show projections of the reconstructed attractor. Notice that the attractor is spread out over the reconstructed space, and that it is being stretched in one direction and folded in the other direction.

Recalling the definition of the Pointwise Dimension from equation (5.2) we can see that there will be some practical difficulties in its evaluation. Firstly, the number of data points, n_d , will have to be finite, and secondly, the limit $r\rightarrow 0$ will have some lower cut-off point. Now, consider equation (5.2) in the form:

$$d = \lim_{n_d \to \infty} \lim_{r \to 0} (D)$$

where

$$D = \frac{\log(P)}{\log(r)}$$

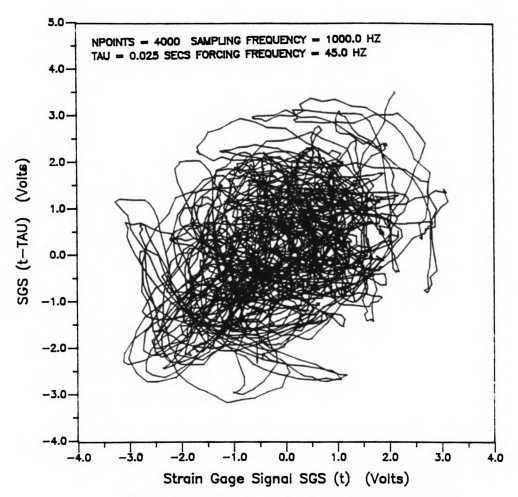


Figure 5.3a: Phase portrait of measured time signal SGS (t) from cantilever beam using the reconstructed coordinates.

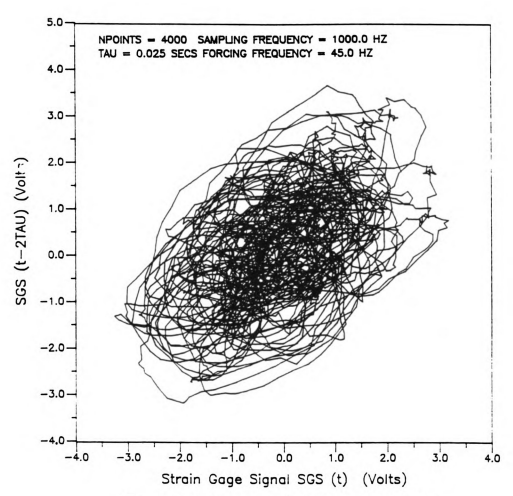


Figure 5.3b: Phase portrait of measured time signal SGS (t) from cantilever beam using the reconstructed coordinates.

and where

$$P = \frac{N_{\overline{x}_0}(r)}{n_d}$$

The first difficulty can be alleviated by taking n_d as large as possible (in our case 40,000 data points) and by calculating P at various reference points, \vec{x}_0 , over the attractor. The various values of P are then averaged and a plot of log (P) vs log (r) constructed. Examples of such a plot are presented in Figure 5.4a for m=3,9 and 15. Referring to this figure, we can clearly see there exists a range of r (represented by solid line) over which the slope of the curve (i.e. d) is non zero. This region is often called the scaling region. The upper bound of this scaling region occurs as r approaches the size of the attractor, and the lower limit occurs when r becomes so small that there are not enough data points within the hypersphere to give a meaningful result. Also note that the scaling region shifts to higher values of radii as the embedding dimension increases. This is due to the fact that the attractor stretches as the phase space dimension increase and therefore the number of data points lying within a set radius decreases.

Figure 5.4b shows the estimated dimension for each embedding space in the range of m = 1 through 15. It is evident that the dimension d reaches an asymptote of approximately d=6.63 when $m\approx15$. This is in agreement with Taken's theorem [1981] previously mentioned in Section 5.1.

Hence

$$d = 6.63$$
 $M = 6$
 $N \ge M+1$
Therefore $N \ge 7$

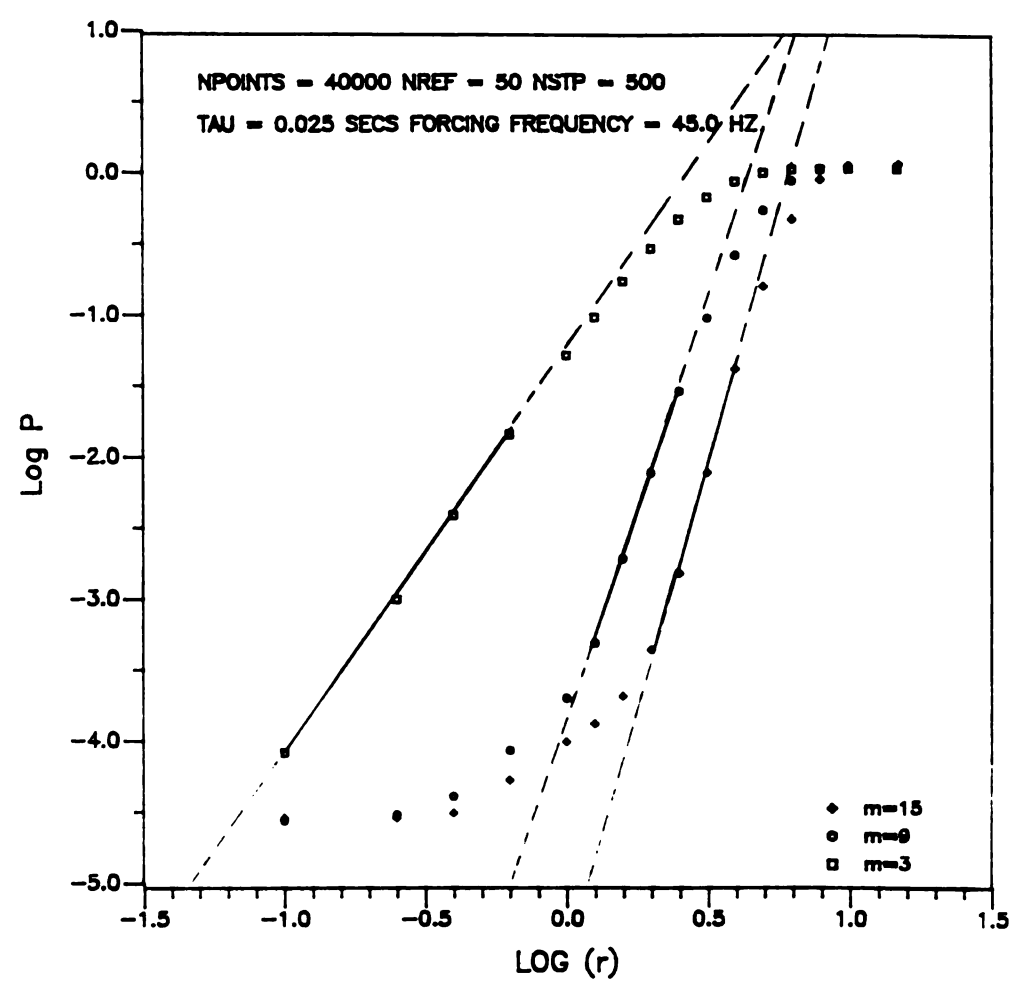


Figure 5.4a: log P plotted against log (r) for m=3,9 and 15.

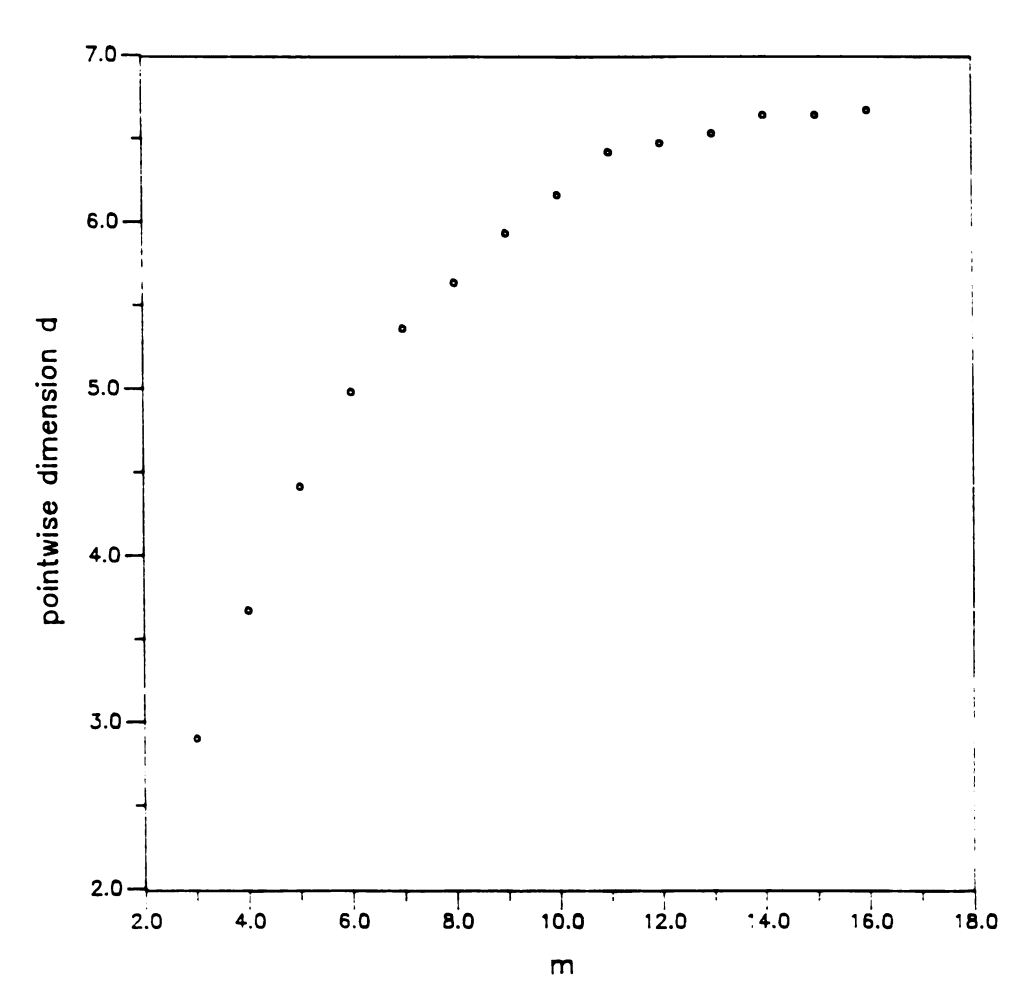


Figure 5.4 b The embedding dimension m plotted against the pointwise dimension of the attractor.

5.5 Conclusions

The minimum number of linearly independent coordinates required to completely describe the dynamics of the cantilever beam, while in this chaotic regime, is 7. Hence it can be modelled mathematically by three orthogonal linear modes which account for 6 of the 7 linearly independent coordinates. The dynamical system equations contain a parametric excitation term which accounts for the 7th coordinate, since time acts as an additional coordinate.

The motion of the beam is chaotic as the pointwise dimension is non-integer.

CHAPTER 6

CONCLUSIONS

The behaviour of a flexible cantilever beam excited by a sinusoidal base excitation in the axial direction has been studied. The governing partial integro-differential equation has been derived assuming the motion to be planar. The equation includes up to third order nonlinear terms arising from large curvature and the associated axial deflections.

The main thrust of the research was to explore, through physical experimentation, the various types of resonant behaviour that the cantilever exhibits. There were found to be two main classifications, viz.

1) Planar Motions,

and

2) Non Planar Motions.

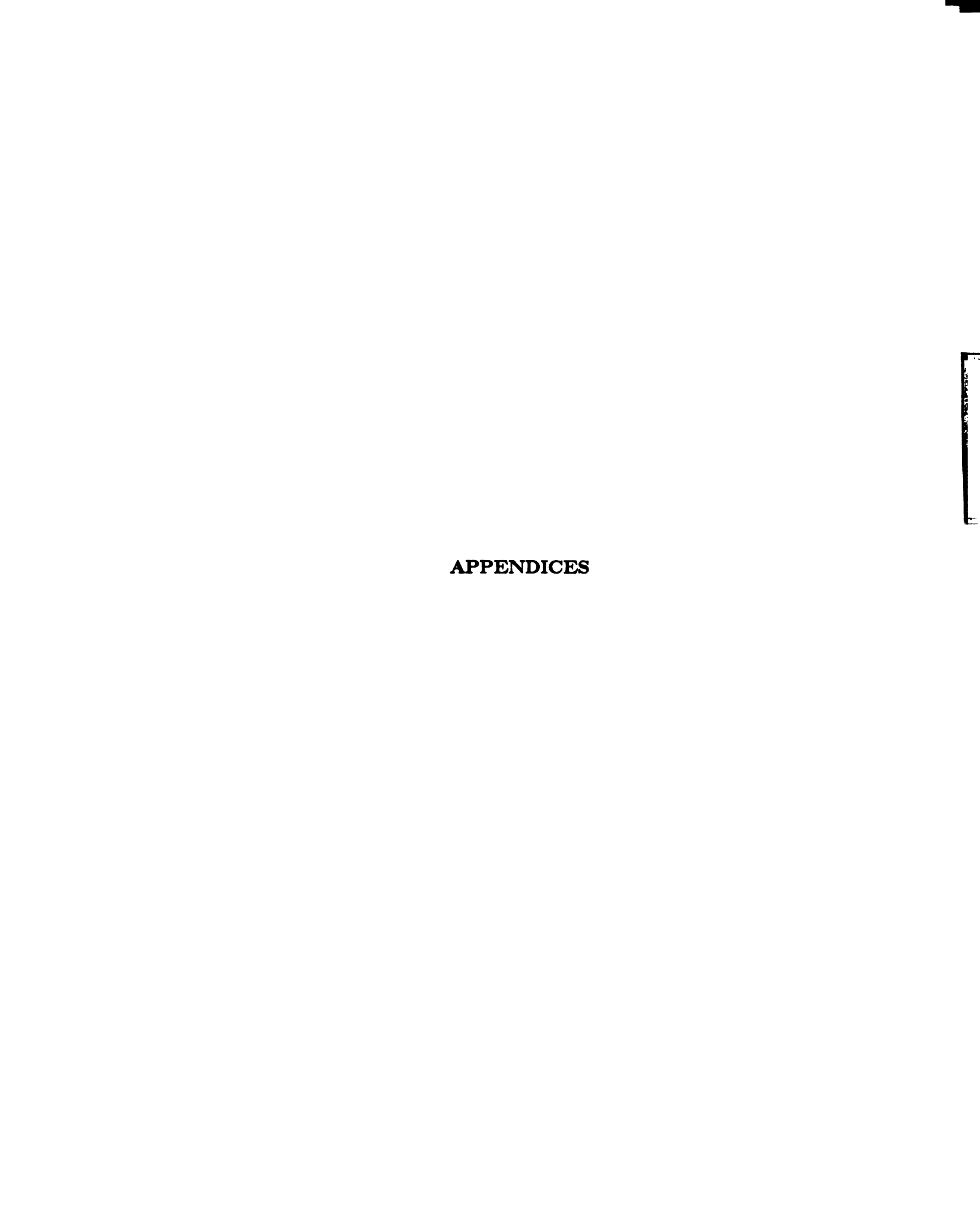
Under classication 1 were observed multi-valued steady-state responses, jump phenomenon, main parametric resonances, multi-mode interactions, almost periodic solutions and finally, very high order sub-harmonic responses. Although a number of these phenomena have received attention in the past, very little work has been reported in the literature on the physical evidence of multi-mode interaction and very high order sub-harmonic responses. These are particularly interesting in that they result in modes being excited at frequencies very far removed from the excitation frequency. The energy put into the system "cascades" down to a lower frequency and results in very large response amplitudes even although the input amplitude is extremely small. If not allowed for at the design stage, this could be potentially a very dangerous situation.

It is recommended that this "cascading" behaviour be studied in more detail.

The partial integro-differential equation obtained in Chapter 2 could be a starting

point for an analytical study of the phenomenon.

Under classification 2 were observed transient chaos, intermittent chaos, and steady-state chaos. The dimension of the steady-state chaos was estimated using Pointwise dimension, and it suggests that the physically observed chaotic response can be modelled mathematically by three orthogonal modes.



APPENDIX A

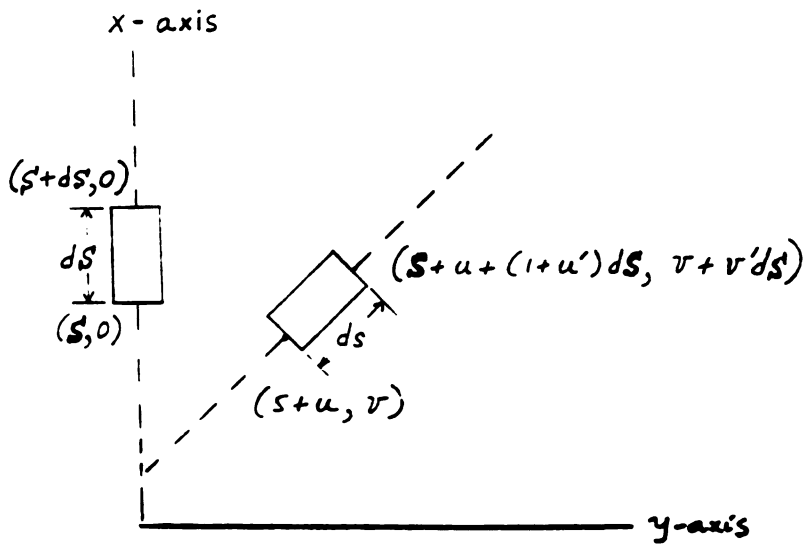


Figure A.1: An element of cantilever beam

Consider an small undeformed element of beam of length ds as shown in above Figure. Referring to the above figure, the deformed length ds of beam element is given by

$$ds = [(1 + u')^2 + v'^2]^{1/2} dS$$

Now the extensional strain is defined as

$$\epsilon(S,t) = \frac{\text{change in length}}{\text{length}}$$

$$= > \epsilon(S,t) = ([(1+u')^2 + v'^2]^{1/2} dS - dS) / dS$$

$$= > \epsilon(S,t) = [(1+u')^2 + v'^2]^{1/2} - 1$$

APPENDIX B

We know from equation (2.6) that

$$\tan\theta = \frac{v'}{1+u'}$$

=>

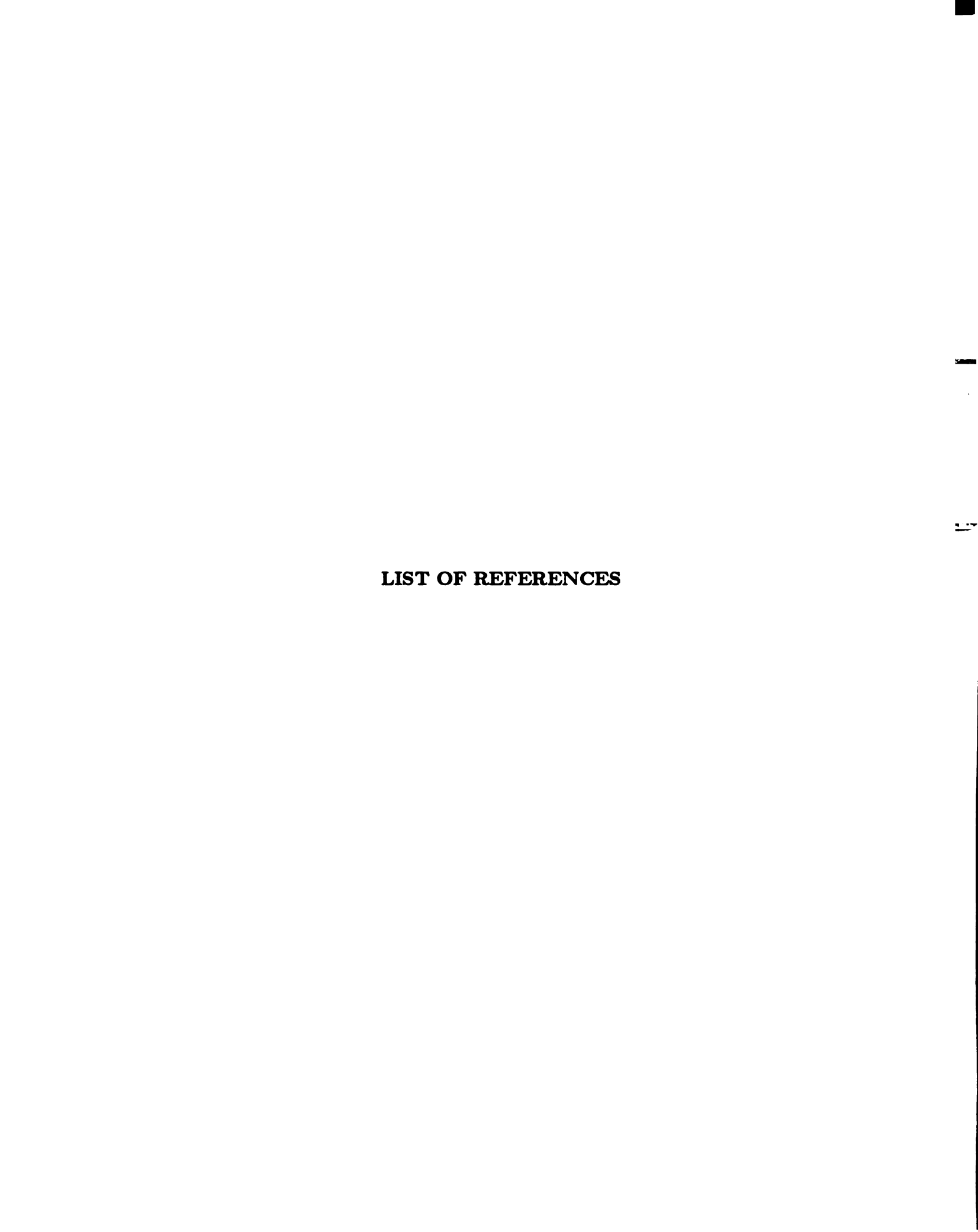
$$\theta = \tan^{-1} \frac{v'}{1+u'}$$

Taking partial derivatives with respect to S, we get

$$\theta' = \frac{v''(1+u')-v'u''}{(1+u')^2+v'^2}$$

Substituting * ' from equation (2.8) into the above relation and dropping higher order terms, we get

$$\theta' = [v''(1 + \frac{1}{2}v'^2)]$$



LIST OF REFERENCES

Alturi, S., [1973] "Nonlinear Vibration of Hinged Beam Including Nonlinear Inertia Effects." J. Appl. Mech., 40, pp 121-126.

Burton, T. D. and Kolowith, M. [1988] "Nonlinear Resonances and Chaos in a Parametrically Excited Flexible Beam", Second Conference on Nonlinear Vibrations, Stability, and Dynamics of Structures and Mechanisms, Virginia Tech., Blacksburg

Barr, A.D.S. [1980] "Some Developments in Parameteric Instability and Nonlinear Vibration." Proceedings of the International Conference on Recent Advances in Structural Dynamics, Southhampton, England.

Berge, P., Pomeau, Y., Vidal, C. [1984]. Order within chaos; Towards a deterministic approach to turbulence, John Wiley and Sons: New York.

Bhashyam, G. R., and Prathap, G. [1980], "Galerkin Finite Element Method for Nonlinear Beam Vibrations." J. of Sound and Vibration, 72 pp 191-203.

Caflisch, R.E., Maddocks, J.H. [1984] "Nonlinear Dynamical Theory of the Elastica." Royal Society of Edinburgh, Proceedings, 99(1-2), pp 1-23.

Crespo da Silva, M.R.M. and Glynn, C.C. [1978a] "Nonlinear Flexural-Flexural-Torsional Dynamics of Inextensional Beams. I - Equations of Motion." J. Struct. Mech. 6(4) pp 437-448

Crespo da Silva, M.R.M. and Glynn, C.C. [1978b] "Nonlinear Flexural-Flexural-Torsional Dynamics of Inextensional Beams. II - Forced Motions." J. Struct. Mech. 6(4) pp 449-461

Dowell, E.H., Traybar, J. and Hodges, D.H. [1977] "An Experimental - Theoretical Correlation Study of Nonlinear Bending and Torsion Deformations of a Cantilever Beam." J. Sound and Vibration 50(4) pp 533-544.

Dugundji, J. and Mukhopadhyay, V. [1973] "Lateral Bending-Torsion Vibrations of a Thin Beam Under Parametric Excitation," J. of Applied Mechanics, Paper #73-APM-13.

Evan-Iwanowski, R.M., [1976] Resonance Oscillations in Mechanical Systems. Elsevier, New York.

Evensen, H.A. and Evan-Iwanowski, R.M. [1966] "Effects of Longitudinal Inertia Upon the Parametric Response of Elastic Folumns," J. of Applied Mech., March, pp 141-148.

Evensen, D.A., [1968] "Nonlinear Vibrations of Beams with Various Boundry Conditions," American Institute of Aeronauics and Astronautics Journal, Vol. 6, pp 370-372.

Farmer, D., Ott, E., and Yorke, J. [1983]. "The Dimension of Chaotic Attractors", *Physica*. ppl53

Goldstein, H. [1980], Classical Mechanics., Addition Wesley Publishing Co.

Grassberger, P. and Procaccia, I [1983b]. "Characterization of Strange Attractors", *Phys. Rev. Lett.*, V.50, No. 5, 346-349

Guckenheimer, J. and Holmes, P. [1986]. Nonlinear Oscillations, Dynamical Systems, and Bifurcations of Vector Fields, Applied Mathematical Sciences No. 42, Springer-Verlag: New York.

Haddow, A.G., Mook, D.T. and Barr, A.D.S., [1984] "Theoretical and Experimental Study of Modal Interaction in a Two-Degree-of-Freedom Structure," J. Sound and Vibration 97(3) pp 451-473.

Haight, E.C. and King, W.W. [1969] "Stability of Parametrically Excited

Vibrations of an Elastic Rod." Proc. Southeastern Conf. Theor. and Applied Mech., 5th, Raleigh, N.C.

Haight, E.C. and King, W.W. [1971] "Stability of Nonlinear Oscillations of an Elastic Rod." J. of Acoustical Soc. Am. 52(3.2) pp 899-911.

Handoo, K.L. and Sundararajan, V. [1971] "Parametric Instability of a Cantilevered Column with End Mass," J. Sound and Vibration 18(1) pp 45-53.

Hartog, J. P. Den, [1956], Mechanical Vibrations, McGraw-Hill Book Company, Inc.

Ho, C.H., Scott, R.A. Eisley, J.G. [1975] "Non-Planar, Nonlinear Oscillations of a Beam - I. Forced Motion," Int. J. Nonlinear Mechanics 9 pp 113-127.

Ho, C.H., Scott, R.A., and Eisley, J.G. [1976] "Non-planar, Nonlinear Oscillations of a Beam. - II Free Motions," J. Sound and Vibration 47(3) pp 333-339.

Holzfuss, J. and Mayer-Kress, G. [1985]. "An Approach to Error-Estimation in the Application of Dimension Algorithms". In Dimensions and Entropies in Chaotic Systems, G. Mayer-Kress (ed.) Springer Verlag, Berlin.

Housner, J. M. and Belvin, W. K. [1986] "Dynamic Response and Collapse of Slender Guyed Booms for Space Application," J. Spacecfart Rocket, 23(1), pp 88-95

Hyer, M., W., [1980] "Nonplanar Motions of a Base Excited Cantilever," International Conference on Recent Advances in Structural Dynamics, Southampton, 2, pp. 621-630

Klewicki, J.C., Hasan, S.M., Haddow, A.G. [1988] "The Documentation and Testing of Computer Programs used in the Estimation of Hausdorff Dimension," *Internal Report*, Department of Mechanical Engineering, Michigan State University.

Luongo, A., Rega, G., Vestroni, F., [1984a] "Accurate Nonlinear equations and Perturbational Solution for the Free Nonplanar Vibration of Inextensional Beams."

2nd International Conference on Recent Advances in Structural Dynamics, Southampton, 1, pp. 341-350

Luongo, A., Rega, G., Vestroni, F., [1986] "On Nonlinear Dynamics of Planar Shear Indeformable Beams," J. Appl. Mech. (53) 619-624.

Mei, C., [1973] "Finite Element Displacement Method for Large Amplitude Free Flexural Vibrations of Beams and Plates," Computers and Structures, Vol. 3, pp. 163-174.

Meirovitch, L. [1967], Analytical Methods in Vibration., Macmillan Company, NewYork

Moon, F.C. [1980] "Experiments on Chaotic Motions of a Forced Nonlinear Oscillator: Strange Attractors." J. Appl. Mech., 47, 638-644.

Moon, F.C. [1987], Chaotic Vibrations An Introduction for Applied Scientists and Engineers, John Wiley & Sons, New York.

Moon, F.C. and Holmes, P.J. [1979] "A Magnetoelastic Strange Attractor." J. Sound and Vibration 65(2) 275-296.

Nayfeh, A.H. Mook, D.T., and Lobitz, D.W., [1974] "Numerical-Petrubation Method for the Nonlinear Analysis of Structural Vibrations," American Institute of Aeronautics and Astronautics Journal, Vol. 12, pp. 1222-1228.

Nayfeh, A.H. and Mook, D.T. [1979] Nonlinear Oscillations, Wiley Interscience, New York.

Ray, J.D., and Bert, C.W., [1969] "Nonlinear Vibrations of a Beam With Pinned Ends," ASME Journal of Engineering for Industry, Vol. 91, pp. 977-1004.

Sathyamoorthy, M. [1982] "Nonlinear Analysis of Beams Part I: Survey of Recent Advances," Shock and Vib. Digest 14(8) pp. 19-35.

Shaw, S.W. [1985] "Forced Vibrations of a Beam with One-Sided Amplitude

Constraint: Theory and Experiment" J. Sounds and Vibration 99(2) 199-212.

Takahshi, K. [1979] "A Method of Stability Analysis for Non-linear Vibration of Beams," J. Sound and Vibration 67(1) 43-54.

Takens, F. [1981] "Detecting Strange Attractors in Turbulence", In Lecture Notes in Mathematics, V. 898, D.A. Rand and L.S. Young (ed.), p. 366, Springer-Verlag, Berlin.

Thompson, W., T., [1965], Theory of Vibration with Applications, Prentice-Hall, Inc., New Jersey

Tseng, W.Y. and Dugundji, J. [1971] "Nonlinear Vibrations of a Buckled Beam under Harmonic Excitation," J. Appl. Mech. June, 467-476.

Wagner, H., [1965] "Large-Amplitude Free Vibrations of a Beam," ASME Journal of Applied Mechanics, pp. 887-892.

Wojnowsky Krieger, S., [1950], "The Effect of an Axial Force on the Vibration of Hinged Bars," ASME Journal of Applied Mechanics, Vol. 17, pp. 35-36.

